Swansea University
Prifysgol Abertawe

Cronfa
Setting Research Free

Cronfa - Swansea University Open Access Repository

Paper:

An unsymmetric 8-node hexahedral element with high distortion tolerance

Pei-Lei Zhou[1],   Song Cen[1, 4, *, †], Jun-Bin Huang[1], Chen-Feng Li [2] , Qun Zhang [3]

[1] *Department of Engineering Mechanics, School of Aerospace Engineering, Tsinghua University, Beijing 100084, China*

[2] *Zienkiewicz Centre for Computational Engineering & Energy Safety Research Institute, College of Engineering, Swansea University, Swansea SA2 8PP, UK*

[3] *INTESIM (Dalian) CO., LTD., Dalian 116023, China*

[4] *Key Laboratory of Applied Mechanics, School of Aerospace Engineering, Tsinghua University, Beijing 100084, China*

SUMMARY

Among all 3D 8-node hexahedral solid elements in current finite element library, the 'best' one can produce good results for bending problems using coarse regular meshes. However, once the mesh is distorted, the accuracy will drop dramatically. And how to solve this problem is still a challenge that remains outstanding. This paper develops an 8-node, 24-DOF (three conventional DOFs per node) hexahedral element based on the virtual work principle, in which two different sets of displacement fields are employed simultaneously to formulate an unsymmetric element stiffness matrix. The first set simply utilizes the formulations of the traditional 8-node tri-linear isoparametric element, while the second set mainly employs the analytical trial functions in terms of 3D oblique coordinates (R, S, T). The resulting element, denoted by US-ATFH8, contains no adjustable factor, and can be used for both isotropic and anisotropic cases. Numerical examples show it can strictly pass both the first-order (constant stress/strain) patch test and the second-order patch test for pure bending, remove the volume locking, and provide the invariance for coordinate rotation. Especially, it is insensitive to various severe mesh distortions.

---

* Corresponding to: Song Cen, Department of Engineering Mechanics, School of Aerospace Engineering, Tsinghua University, Beijing 100084, China

† E-mail: censong@tsinghua.edu.cn

1. INTRODUCTION

Because of relatively higher accuracy and lower computation cost, 8-node hexahedral isoparametric element is often preferred in analysis of 3D problems [1]. However, for traditional tri-linear isoparametric element, when dealing with solids and structures with complicated loadings or geometries, full integration model may suffer from various locking problems and will be very sensitive to mesh distortions, while reduced integration model may appear hourglass phenomena or lead to incorrect results. Among all 3D 8-node hexahedral solid elements in current finite element library, some incompatible elements [1-5] are usually considered as the models with the best precision because they can produce good results for bending problems using very coarse regular meshes. However, once the mesh is distorted, the accuracy will drop dramatically again. This is a living example of the sensitivity problem to mesh distortion, which is the core inherent difficulty existing in finite element methods. And how to solve this problem is still a challenge that remains outstanding. Actually, the same difficulty is also hard to be overcome even for 2D problems. MacNeal has proved that any 4-node, 8-DOF quadrilateral membrane isoparametric element of trapezoidal shape must either lock in pure bending tests or fail to pass constant stress/strain patch tests [6], and the similar limitation can be generalized to 3D 8-node hexahedral finite elements [7]. It almost closes out further effort to design new element models with high distortion resistance.

For past 60 years, numerous efforts have been made to improve performance and capacity of finite elements, such as the incompatible displacement methods proposed by Wilson *et al.* [2] and the modified version by Taylor *et al.* [3], the reduced or selective reduced integration patterns [8-10] and the corresponding hourglass control techniques [11-14], the enhanced assumed strain (EAS) methods [4, 5, 15, 16], the hybrid element methods [17, 18], the analytical interpolation method [19], the finite element-meshfree combination method [20], and so on.

However, it seems that no element mentioned above is truly beyond the limitation shown by MacNeal [6, 7].

Lee and Bathe [21] pointed out that the nonlinear transformation relationship between parametric and physical coordinates may be one of the reasons that cause the sensitivity problem to mesh distortions. In order to avoid the troubles caused by this nonlinear relationship, Long *et al.* successively established three forms of 2D quadrilateral area coordinate methods (QACM-I, QACM-II and QACM-III) [22-26] and a 3D hexahedral volume coordinate method (HVCM) [27], in which the transformations between these new local coordinates and the Cartesian (physical) coordinates are always linear, respectively. Subsequently, a series of new quadrilateral plane membrane elements [25, 26, 28-33] and 3D hexahedral elements [27] were developed. Although many elements greatly improve the distortion resistance for bending tests, all of them fail to strictly pass the constant stress/strain (C_0) patch tests. So, their convergence raised some queries and discussions [34, 35]. Cen *et al.* [29] and Chen *et al.* [36] tried to make them pass the C_0 patch test, but the distortion resistance will be destroyed again for bending tests.

For developing distortion-immune elements, some researchers began to look for new formulations from other theoretical space. Rajendran *et al.* [37-42] adopted the virtual work principle to establish a kind of unsymmetric finite element method, in which the test and the trial functions for displacement fields are different and the resulting element stiffness matrix is unsymmetric. For test functions, the conventional shape functions of isoparametric elements are selected to exactly satisfy the minimum inter- as well as intra-element displacement continuity requirements; and for trial functions, the polynomials in terms of Cartesian (physical) coordinates are chosen to satisfy the completeness requirements in physical space. Since there is no Jacobian determinant in the final formula for evaluating the element stiffness matrix, the resulting elements can still perform well even when they are severely distorted. However, their method is only effective for constructing high-order elements, such as 8-node plane quadrilateral element US-QUAD8 [37] and 20-node 3D hexahedral element US-HEXA20 [38]. Furthermore, because the number of element DOFs usually does not equal to the number of items for a complete

polynomial in terms of Cartesian coordinates, interpolation failure may take place when the element is distorted to certain shapes, and rotational frame dependence may also appear [43]. So, they are not convenient and effective for practical applications. Cen *et al*. [44] developed a new 8-node unsymmetric plane element US-ATFQ8 by introducing analytical trial functions and generalized conforming conditions. This element can overcome all above defects and even produce exact solutions in linear bending problems (third-order patch test).

Recently, some significant progresses have also been made for developing low-order elements. Cen *et al.* [45] successfully formulated an unsymmetric 4-node, 8-DOF plane element. The key technique is that the second displacement field set (trial functions) employs a composite coordinate interpolation scheme with analytical trial function method, in which the items 1, *x*, *y* and two sets of analytical solutions for pure bending state in terms of the second form of quadrilateral area coordinates (QACM-II) are applied together. The resulting element US-ATFQ4, which can be used for both isotropic and anisotropic cases, exhibits amazing performance in rigorous tests. It can satisfy both the classical first-order (constant stress/strain) patch test and the second-order patch test for pure bending, and is insensitive to various severe mesh distortions. Due to the isotropy of the natural local coordinate QACM-II, US-ATFQ4 can provide the invariance for the coordinate rotation. The appearance of this element seems that the limitation defined by MacNeal's theorem can be broken through. Almost at the same time, Xie *et al*. [46] also utilized similar procedure developed a 4-node plane element TQ4 and an 8-node hexahedral element TH8. The major different is that they used a kind of local oblique coordinate method defined by Yuan *et al*. [47, 48] together with Cartesian and isoparametric coordinates in their interpolation formulae. However, these two elements can be used only for isotropic problems. Furthermore, an adjustable factor β varying from 0.01 to 0.0001 ($\beta = 0.01$ was adopted by [46]) is introduced into the interpolation matrix of element TH8 for enhancing the element accuracy. In fact, because this factor has no definite physical significance, incorrect results may appear if the factor is not appropriate (see Section 4.2 and Tables 4 and 6).

The purpose of this paper is to present an 8-node hexahedral element with high distortion resistance as well as no obvious numerical defects. First, nine sets of analytical general solutions for linear stresses, linear strains and quadratic displacements in terms of 3D local oblique coordinates (R, S, T) [47, 48], which are not found in other literatures, are derived. These analytical solutions are also the Trefftz solutions [49]. Then, a new 8-node hexahedral element is developed based on the virtual work principle, in which two different sets of displacement fields are employed simultaneously to formulate an unsymmetric element stiffness matrix. The first set simply utilizes the formulations of the 8-node tri-linear isoparametric element, while the second set mainly employs the analytical trial functions in terms of 3D local oblique coordinates. Because the relationship between the local oblique and Cartesian coordinates is always linear, and there is no Jacobian determinant needed for computing the element stiffness matrix, the new element is expected to be insensitive to mesh distortion. The resulting element, denoted by US-ATFH8, contains no adjustable factor, and can be used for both isotropic and anisotropic cases. Numerical examples show it can exactly pass both the first-order (constant stress/strain) patch test and the second-order patch test for pure bending, remove the volume locking, and provide the invariance for coordinate rotation. Especially, it is insensitive to various severe mesh distortions.

2. ANALYTICAL GENERAL SOLUTIONS IN TERMS OF 3D OBLIQUE COORDINATES

As described in previous section, in order to construct finite element models insensitive to mesh distortion, a local coordinate system which is linearly related to the global Cartesian coordinate system should be considered. For 3D problems, the most feasible one is the oblique (skew) coordinate system defined by Yuan *et al.* [47, 48].

2.1. Definition of 3D oblique coordinate system [47, 48]

For an 8-node hexahedral element shown in Figure 1, the Cartesian coordinates (x, y, z) can be expressed in terms of the isoparametric coordinates (ξ, η, ζ) as

$$\begin{Bmatrix} x \\ y \\ z \end{Bmatrix} = \sum_{i=1}^{8} \bar{N}_i \begin{Bmatrix} x_i \\ y_i \\ z_i \end{Bmatrix} = \begin{Bmatrix} x_0 + \bar{a}_1\xi + \bar{a}_2\eta + \bar{a}_3\zeta + \bar{a}_4\xi\eta + \bar{a}_5\eta\zeta + \bar{a}_6\xi\zeta + \bar{a}_7\xi\eta\zeta \\ y_0 + \bar{b}_1\xi + \bar{b}_2\eta + \bar{b}_3\zeta + \bar{b}_4\xi\eta + \bar{b}_5\eta\zeta + \bar{b}_6\xi\zeta + \bar{b}_7\xi\eta\zeta \\ z_0 + \bar{c}_1\xi + \bar{c}_2\eta + \bar{c}_3\zeta + \bar{c}_4\xi\eta + \bar{c}_5\eta\zeta + \bar{c}_6\xi\zeta + \bar{c}_7\xi\eta\zeta \end{Bmatrix}, \tag{1}$$

with

$$\bar{N}_i = \frac{1}{8}(1 + \xi_i\xi)(1 + \eta_i\eta)(1 + \zeta_i\zeta) \qquad i = (1,2,...,8), \tag{2}$$

$$\begin{Bmatrix} x_0 \\ y_0 \\ z_0 \end{Bmatrix} = \frac{1}{8}\sum_{i=1}^{8} \begin{Bmatrix} x_i \\ y_i \\ z_i \end{Bmatrix}, \quad \begin{Bmatrix} \bar{a}_1 \\ \bar{b}_1 \\ \bar{c}_1 \end{Bmatrix} = \frac{1}{8}\sum_{i=1}^{8} \xi_i \begin{Bmatrix} x_i \\ y_i \\ z_i \end{Bmatrix}, \quad \begin{Bmatrix} \bar{a}_2 \\ \bar{b}_2 \\ \bar{c}_2 \end{Bmatrix} = \frac{1}{8}\sum_{i=1}^{8} \eta_i \begin{Bmatrix} x_i \\ y_i \\ z_i \end{Bmatrix}, \quad \begin{Bmatrix} \bar{a}_3 \\ \bar{b}_3 \\ \bar{c}_3 \end{Bmatrix} = \frac{1}{8}\sum_{i=1}^{8} \zeta_i \begin{Bmatrix} x_i \\ y_i \\ z_i \end{Bmatrix}, \tag{3}$$

in which (ξ_i, η_i, ζ_i) and (x_i, y_i, z_i) $(i=1\sim8)$ are the isoparametric and Cartesian coordinates of the eight corner nodes, respectively.

Yuan *et al*. [47, 48] defined a kind of 3D oblique coordinates (R, S, T) as follows

$$\begin{Bmatrix} R \\ S \\ T \end{Bmatrix} = (\mathbf{J}_0^{-1})^{\mathrm{T}} \left(\begin{Bmatrix} x \\ y \\ z \end{Bmatrix} - \begin{Bmatrix} x \\ y \\ z \end{Bmatrix}_{\xi=\eta=\zeta=0} \right) = \frac{1}{J_0} \begin{bmatrix} a_1 & b_1 & c_1 \\ a_2 & b_2 & c_2 \\ a_3 & b_3 & c_3 \end{bmatrix} \begin{Bmatrix} x - x_0 \\ y - y_0 \\ z - z_0 \end{Bmatrix}, \tag{4}$$

where $\mathbf{J}_0$ denotes the Jacobian matrix at the origin of the isoparametric coordinates $(\xi, \eta, \zeta)=(0, 0, 0)$,

$$\mathbf{J}_0 = \begin{bmatrix} \dfrac{\partial x}{\partial \xi} & \dfrac{\partial y}{\partial \xi} & \dfrac{\partial z}{\partial \xi} \\ \dfrac{\partial x}{\partial \eta} & \dfrac{\partial y}{\partial \eta} & \dfrac{\partial z}{\partial \eta} \\ \dfrac{\partial x}{\partial \zeta} & \dfrac{\partial y}{\partial \zeta} & \dfrac{\partial z}{\partial \zeta} \end{bmatrix}_{\xi=\eta=\zeta=0} = \begin{bmatrix} \bar{a}_1 & \bar{b}_1 & \bar{c}_1 \\ \bar{a}_2 & \bar{b}_2 & \bar{c}_2 \\ \bar{a}_3 & \bar{b}_3 & \bar{c}_3 \end{bmatrix}, \tag{5}$$

$$\begin{aligned} J_0 = |\mathbf{J}_0| &= \bar{a}_1(\bar{b}_2\bar{c}_3 - \bar{b}_3\bar{c}_2) + \bar{a}_2(\bar{b}_3\bar{c}_1 - \bar{b}_1\bar{c}_3) + \bar{a}_3(\bar{b}_1\bar{c}_2 - \bar{b}_2\bar{c}_1) \\ &= \bar{a}_1 a_1 + \bar{a}_2 a_2 + \bar{a}_3 a_3 = \bar{b}_1 b_1 + \bar{b}_2 b_2 + \bar{b}_3 b_3 = \bar{c}_1 c_1 + \bar{c}_2 c_2 + \bar{c}_3 c_3 \end{aligned}, \tag{6}$$

$$\begin{aligned} a_1 &= \bar{b}_2\bar{c}_3 - \bar{b}_3\bar{c}_2, & b_1 &= \bar{a}_3\bar{c}_2 - \bar{a}_2\bar{c}_3, & c_1 &= \bar{a}_2\bar{b}_3 - \bar{a}_3\bar{b}_2 \\ a_2 &= \bar{b}_3\bar{c}_1 - \bar{b}_1\bar{c}_3, & b_2 &= \bar{a}_1\bar{c}_3 - \bar{a}_3\bar{c}_1, & c_2 &= \bar{a}_3\bar{b}_1 - \bar{a}_1\bar{b}_3 \\ a_3 &= \bar{b}_1\bar{c}_2 - \bar{b}_2\bar{c}_1, & b_3 &= \bar{a}_2\bar{c}_1 - \bar{a}_1\bar{c}_2, & c_3 &= \bar{a}_1\bar{b}_2 - \bar{a}_2\bar{b}_1 \end{aligned}. \tag{7}$$

It can be easily found that the relationship of the oblique coordinates (R, S, T) and the Cartesian coordinates (x, y, z) is always linear. As shown in Figure 1, (R, S, T) and the isoparametric coordinates (ξ, η, ζ) share the same directions, respectively, and their origins also coincide with each other.

The transformation of first-order derivatives is

$$
\begin{Bmatrix} \dfrac{\partial}{\partial x} \\[2mm] \dfrac{\partial}{\partial y} \\[2mm] \dfrac{\partial}{\partial z} \end{Bmatrix} = \begin{bmatrix} \dfrac{\partial R}{\partial x} & \dfrac{\partial S}{\partial x} & \dfrac{\partial T}{\partial x} \\[2mm] \dfrac{\partial R}{\partial y} & \dfrac{\partial S}{\partial y} & \dfrac{\partial T}{\partial y} \\[2mm] \dfrac{\partial R}{\partial z} & \dfrac{\partial S}{\partial z} & \dfrac{\partial T}{\partial z} \end{bmatrix} \begin{Bmatrix} \dfrac{\partial}{\partial R} \\[2mm] \dfrac{\partial}{\partial S} \\[2mm] \dfrac{\partial}{\partial T} \end{Bmatrix} = \frac{1}{J_0} \begin{bmatrix} a_1 & a_2 & a_3 \\ b_1 & b_2 & b_3 \\ c_1 & c_2 & c_3 \end{bmatrix} \begin{Bmatrix} \dfrac{\partial}{\partial R} \\[2mm] \dfrac{\partial}{\partial S} \\[2mm] \dfrac{\partial}{\partial T} \end{Bmatrix} . \tag{8}
$$

And the transformation of second-order derivatives is

$$
\begin{Bmatrix} \dfrac{\partial^2}{\partial x^2} \\[2mm] \dfrac{\partial^2}{\partial y^2} \\[2mm] \dfrac{\partial^2}{\partial z^2} \\[2mm] \dfrac{\partial^2}{\partial x \partial y} \\[2mm] \dfrac{\partial^2}{\partial x \partial z} \\[2mm] \dfrac{\partial^2}{\partial y \partial z} \end{Bmatrix} = \frac{1}{J_0^2} \begin{bmatrix} a_1^2 & a_2^2 & a_3^2 & 2a_1 a_2 & 2a_1 a_3 & 2a_2 a_3 \\ b_1^2 & b_2^2 & b_3^2 & 2b_1 b_2 & 2b_1 b_3 & 2b_2 b_3 \\ c_1^2 & c_2^2 & c_3^2 & 2c_1 c_2 & 2c_1 c_3 & 2c_2 c_3 \\ a_1 b_1 & a_2 b_2 & a_3 b_3 & a_1 b_2 + a_2 b_1 & a_1 b_3 + a_3 b_1 & a_2 b_3 + a_3 b_2 \\ a_1 c_1 & a_2 c_2 & a_3 c_3 & a_1 c_2 + a_2 c_1 & a_1 c_3 + a_3 c_1 & a_2 c_3 + a_3 c_2 \\ b_1 c_1 & b_2 c_2 & b_3 c_3 & b_1 c_2 + b_2 c_1 & b_1 c_3 + b_3 c_1 & b_2 c_3 + b_3 c_2 \end{bmatrix} \begin{Bmatrix} \dfrac{\partial^2}{\partial R^2} \\[2mm] \dfrac{\partial^2}{\partial S^2} \\[2mm] \dfrac{\partial^2}{\partial T^2} \\[2mm] \dfrac{\partial^2}{\partial R \partial S} \\[2mm] \dfrac{\partial^2}{\partial R \partial T} \\[2mm] \dfrac{\partial^2}{\partial S \partial T} \end{Bmatrix} . \tag{9}
$$

2.2. The analytical general solutions in terms of 3D oblique coordinate system

In order to improve element performance, the analytical solutions of stresses, strains, or displacements satisfying governing equations in elasticity are often taken as the trial functions in some finite element methods, such as the Trefftz finite element method [49] and the hybrid stress-function element method proposed by Cen *et al*. [50-55]. It is also noteworthy that the usage of the analytical solutions in terms of the local coordinates [32, 45] may eliminate directional dependence problem. In this section, nine sets of analytical general solutions for linear stresses, linear strains and quadratic displacements in terms of 3D local oblique coordinates will be derived.

For three-dimensional problems without body forces, the homogeneous equilibrium equations in the oblique coordinate system are given by

$$
\begin{cases}
\dfrac{\partial \sigma_R}{\partial R} + \dfrac{\partial \tau_{SR}}{\partial S} + \dfrac{\partial \tau_{TR}}{\partial T} = 0 \\[2mm]
\dfrac{\partial \sigma_S}{\partial S} + \dfrac{\partial \tau_{TS}}{\partial T} + \dfrac{\partial \tau_{RS}}{\partial R} = 0 \\[2mm]
\dfrac{\partial \sigma_T}{\partial T} + \dfrac{\partial \tau_{RT}}{\partial R} + \dfrac{\partial \tau_{ST}}{\partial S} = 0
\end{cases}
\tag{10}
$$

The first 27 sets of analytical solutions for above stresses in terms of 3D oblique coordinate system are listed in Table 1, in which the first 3 sets, 4th to 12th sets and 13th to 27th sets are related to the rigid body, the linear and the quadratic displacement modes, respectively. Since the constant stress solutions will not be used later, their explicit forms are not given in the table.

According to equation (4), the stress components in Cartesian coordinates (x, y, z) can be expressed by the stress components in oblique coordinates (R, S, T):

$$
\begin{bmatrix}
\sigma_x & \tau_{xy} & \tau_{zx} \\
\tau_{xy} & \sigma_y & \tau_{yz} \\
\tau_{zx} & \tau_{yz} & \sigma_z
\end{bmatrix}
=
\begin{bmatrix}
\bar{a}_1 & \bar{b}_1 & \bar{c}_1 \\
\bar{a}_2 & \bar{b}_2 & \bar{c}_2 \\
\bar{a}_3 & \bar{b}_3 & \bar{c}_3
\end{bmatrix}^{\mathrm{T}}
\begin{bmatrix}
\sigma_R & \tau_{RS} & \tau_{RT} \\
\tau_{RS} & \sigma_S & \tau_{ST} \\
\tau_{RT} & \tau_{ST} & \sigma_T
\end{bmatrix}
\begin{bmatrix}
\bar{a}_1 & \bar{b}_1 & \bar{c}_1 \\
\bar{a}_2 & \bar{b}_2 & \bar{c}_2 \\
\bar{a}_3 & \bar{b}_3 & \bar{c}_3
\end{bmatrix},
\tag{11}
$$

i.e.

$$
\begin{Bmatrix}
\sigma_x \\ \sigma_y \\ \sigma_z \\ \tau_{xy} \\ \tau_{yz} \\ \tau_{zx}
\end{Bmatrix}
=
\begin{bmatrix}
\bar{a}_1^2 & \bar{a}_2^2 & \bar{a}_3^2 & 2\bar{a}_1\bar{a}_2 & 2\bar{a}_2\bar{a}_3 & 2\bar{a}_1\bar{a}_3 \\
\bar{b}_1^2 & \bar{b}_2^2 & \bar{b}_3^2 & 2\bar{b}_1\bar{b}_2 & 2\bar{b}_2\bar{b}_3 & 2\bar{b}_1\bar{b}_3 \\
\bar{c}_1^2 & \bar{c}_2^2 & \bar{c}_3^2 & 2\bar{c}_1\bar{c}_2 & 2\bar{c}_2\bar{c}_3 & 2\bar{c}_1\bar{c}_3 \\
\bar{a}_1\bar{b}_1 & \bar{a}_2\bar{b}_2 & \bar{a}_3\bar{b}_3 & \bar{a}_1\bar{b}_2+\bar{a}_2\bar{b}_1 & \bar{a}_2\bar{b}_3+\bar{a}_3\bar{b}_2 & \bar{a}_1\bar{b}_3+\bar{a}_3\bar{b}_1 \\
\bar{b}_1\bar{c}_1 & \bar{b}_2\bar{c}_2 & \bar{b}_3\bar{c}_3 & \bar{b}_1\bar{c}_2+\bar{b}_2\bar{c}_1 & \bar{b}_2\bar{c}_3+\bar{b}_3\bar{c}_2 & \bar{b}_1\bar{c}_3+\bar{b}_3\bar{c}_1 \\
\bar{a}_1\bar{c}_1 & \bar{a}_2\bar{c}_2 & \bar{a}_3\bar{c}_3 & \bar{a}_1\bar{c}_2+\bar{a}_2\bar{c}_1 & \bar{a}_2\bar{c}_3+\bar{a}_3\bar{c}_2 & \bar{a}_1\bar{c}_3+\bar{a}_3\bar{c}_1
\end{bmatrix}
\begin{Bmatrix}
\sigma_R \\ \sigma_S \\ \sigma_T \\ \tau_{RS} \\ \tau_{ST} \\ \tau_{RT}
\end{Bmatrix}.
\tag{12}
$$

Then, the strains in Cartesian coordinate system can be obtained by following stress-strain relations (generalized Hooke law):

$$\boldsymbol{\varepsilon} = \begin{Bmatrix} \varepsilon_x \\ \varepsilon_y \\ \varepsilon_z \\ \gamma_{xy} \\ \gamma_{yz} \\ \gamma_{zx} \end{Bmatrix} = \frac{1}{E} \begin{bmatrix} 1 & -\mu & -\mu & 0 & 0 & 0 \\ -\mu & 1 & -\mu & 0 & 0 & 0 \\ -\mu & -\mu & 1 & 0 & 0 & 0 \\ 0 & 0 & 0 & 2(1+\mu) & 0 & 0 \\ 0 & 0 & 0 & 0 & 2(1+\mu) & 0 \\ 0 & 0 & 0 & 0 & 0 & 2(1+\mu) \end{bmatrix} \begin{Bmatrix} \sigma_x \\ \sigma_y \\ \sigma_z \\ \tau_{xy} \\ \tau_{yz} \\ \tau_{zx} \end{Bmatrix} = \mathbf{C}\boldsymbol{\sigma} \text{, for isotropic case;} \quad (13a)$$

$$\boldsymbol{\varepsilon} = \begin{Bmatrix} \varepsilon_x \\ \varepsilon_y \\ \varepsilon_z \\ \gamma_{xy} \\ \gamma_{yz} \\ \gamma_{zx} \end{Bmatrix} = \begin{bmatrix} C_{11} & C_{12} & C_{13} & C_{14} & C_{15} & C_{16} \\ C_{21} & C_{22} & C_{23} & C_{24} & C_{25} & C_{26} \\ C_{31} & C_{32} & C_{33} & C_{34} & C_{35} & C_{36} \\ C_{41} & C_{42} & C_{43} & C_{44} & C_{45} & C_{46} \\ C_{51} & C_{52} & C_{53} & C_{54} & C_{55} & C_{56} \\ C_{61} & C_{62} & C_{63} & C_{64} & C_{65} & C_{66} \end{bmatrix} \begin{Bmatrix} \sigma_x \\ \sigma_y \\ \sigma_z \\ \tau_{xy} \\ \tau_{yz} \\ \tau_{zx} \end{Bmatrix} = \mathbf{C}\boldsymbol{\sigma} \text{,} \qquad \text{for anisotropic case,} \quad (13b)$$

where $\mathbf{C}$ is the elasticity matrix of compliances; E and μ are Young's modulus and Poisson's ratio, respectively.

Thus, these strains can also be expressed by the stress components in local oblique coordinates by substituting Equation (12) into (13).

Finally, by using Equation (8) and integrating following geometrical equations

$$\begin{cases} \varepsilon_x = \dfrac{\partial u}{\partial x}, & \varepsilon_y = \dfrac{\partial v}{\partial y}, & \varepsilon_z = \dfrac{\partial w}{\partial z} \\[2mm] \gamma_{xy} = \dfrac{\partial u}{\partial y} + \dfrac{\partial v}{\partial x}, & \gamma_{yz} = \dfrac{\partial v}{\partial z} + \dfrac{\partial w}{\partial y}, & \gamma_{zx} = \dfrac{\partial u}{\partial z} + \dfrac{\partial w}{\partial x} \end{cases} \tag{14}$$

the displacements u, v and w in Cartesian coordinate system can be solved.

Following above procedure, the analytical general solutions of stresses, strains and displacements in the global coordinate system, but in terms of the local oblique coordinates R, S and T, can be obtained.

Only nine sets ($i=13\sim21$) of the analytical general solutions for local linear stresses in Table 1 related to pure bending and twisting states will be considered in the new finite element formulations, which are given in appendix A.

3. CONSTRUCTION OF A NEW UNSYMMETRIC 8-NODE HEXAHEDRAL ELEMENT US-ATFH8

For a three-dimensional 8-node, 24-DOF (3 DOFs per node) finite element model shown in Figure 2, the virtual work principle [37, 38] can be written as

$$\iiint_{V^e} \delta\tilde{\boldsymbol{\varepsilon}}^{\mathrm{T}}\hat{\boldsymbol{\sigma}}\mathrm{d}V - \iiint_{V^e} \delta\overline{\mathbf{u}}^{\mathrm{T}}\mathbf{b}\mathrm{d}V - \int_{\Gamma^e} \delta\overline{\mathbf{u}}^{\mathrm{T}}\mathbf{T}\mathrm{d}\Gamma - \delta\overline{\mathbf{u}}_c^{\mathrm{T}}\mathbf{f}_c = 0, \tag{15}$$

in which V^e denotes the element volume; Γ^e represents the element boundary face; $\hat{\boldsymbol{\sigma}}$ is the real stress vector of the element; $\mathbf{b}$, $\mathbf{T}$ and $\mathbf{f}_c$ are the real body, surface and concentrated forces of the element, respectively; $\delta\overline{\mathbf{u}}_c$ is the vector of virtual displacements at the points of the concentrated forces; $\delta\overline{\mathbf{u}}$ is the virtual displacement fields and $\delta\tilde{\boldsymbol{\varepsilon}}$ is the corresponding virtual strain fields.

First, the virtual displacement fields $\delta\overline{\mathbf{u}} = [\delta u \quad \delta v \quad \delta w]^{\mathrm{T}}$ should satisfy exactly the minimum inter- as well as intra-element displacement continuity requirements. So, they can be assumed as

$$\delta\overline{\mathbf{u}} = \overline{\mathbf{N}}\delta\mathbf{q}^e, \tag{16}$$

where

$$\delta\mathbf{q}^e = [\delta u_1 \quad \delta v_1 \quad \delta w_1 \quad \cdots \quad \delta u_8 \quad \delta v_8 \quad \delta w_8]^{\mathrm{T}}, \tag{17}$$

$$\overline{\mathbf{N}} = \begin{bmatrix} \overline{N}_1 & 0 & 0 & \cdots & \overline{N}_8 & 0 & 0 \\ 0 & \overline{N}_1 & 0 & \cdots & 0 & \overline{N}_8 & 0 \\ 0 & 0 & \overline{N}_1 & \cdots & 0 & 0 & \overline{N}_8 \end{bmatrix}, \tag{18}$$

in which δu_i, δv_i and δw_i ($i = 1 \sim 8$) are the nodal virtual displacements along x-, y- and z- directions, respectively; $\overline{N}_i$ ($i = 1 \sim 8$) are just the shape functions of the traditional 8-node tri-linear isoparametric element that satisfy all continuity requirements, and have been given by Equation (2).

Thus, the corresponding virtual strain fields $\delta\tilde{\boldsymbol{\varepsilon}}$ are

$$\delta\tilde{\boldsymbol{\varepsilon}} = [\delta\overline{\varepsilon}_x \quad \delta\overline{\varepsilon}_y \quad \delta\overline{\varepsilon}_z \quad \delta\overline{\gamma}_{xy} \quad \delta\overline{\gamma}_{yz} \quad \delta\overline{\gamma}_{zx}]^{\mathrm{T}} = \overline{\mathbf{B}}\delta\mathbf{q}^e, \tag{19}$$

where $\overline{\mathbf{B}}$ is the strain matrix of the traditional 8-node tri-linear isoparametric element,

$$\overline{\mathbf{B}} = \mathbf{L}\overline{\mathbf{N}} = \frac{1}{|\mathbf{J}|}\overline{\mathbf{B}}^*, \tag{20}$$

with

$$\mathbf{L} = \begin{bmatrix} \dfrac{\partial}{\partial x} & 0 & 0 & \dfrac{\partial}{\partial y} & 0 & \dfrac{\partial}{\partial z} \\ 0 & \dfrac{\partial}{\partial y} & 0 & \dfrac{\partial}{\partial x} & \dfrac{\partial}{\partial z} & 0 \\ 0 & 0 & \dfrac{\partial}{\partial z} & 0 & \dfrac{\partial}{\partial y} & \dfrac{\partial}{\partial x} \end{bmatrix}^{\mathrm{T}}, \tag{21}$$

and $|\mathbf{J}|$ is the Jacobian determinant,

$$|\mathbf{J}| = \begin{vmatrix} \dfrac{\partial x}{\partial \xi} & \dfrac{\partial y}{\partial \xi} & \dfrac{\partial z}{\partial \xi} \\ \dfrac{\partial x}{\partial \eta} & \dfrac{\partial y}{\partial \eta} & \dfrac{\partial z}{\partial \eta} \\ \dfrac{\partial x}{\partial \zeta} & \dfrac{\partial y}{\partial \zeta} & \dfrac{\partial z}{\partial \zeta} \end{vmatrix}, \tag{22}$$

$$x = \sum_{i=1}^{8} \overline{N}_i x_i, \qquad y = \sum_{i=1}^{8} \overline{N}_i y_i, \qquad z = \sum_{i=1}^{8} \overline{N}_i z_i. \tag{23}$$

Second, assume that the real stresses $\hat{\boldsymbol{\sigma}}$ in Equation (15) are derived from the following assumed

displacement fields expressed in terms of the local oblique coordinates R, S and T;

$$\hat{\mathbf{u}} = \begin{Bmatrix} \hat{u} \\ \hat{v} \\ \hat{w} \end{Bmatrix} = \mathbf{P}\boldsymbol{\alpha} = \begin{bmatrix} 1 & 0 & 0 & R & 0 & 0 & S & 0 & 0 & T & 0 & 0 & U_{13} & \cdots & U_{21} & RST & 0 & 0 \\ 0 & 1 & 0 & 0 & R & 0 & 0 & S & 0 & 0 & T & 0 & V_{13} & \cdots & V_{21} & 0 & RST & 0 \\ 0 & 0 & 1 & 0 & 0 & R & 0 & 0 & S & 0 & 0 & T & W_{13} & \cdots & W_{21} & 0 & 0 & RST \end{bmatrix} \begin{Bmatrix} \alpha_1 \\ \vdots \\ \alpha_{24} \end{Bmatrix}, \tag{24}$$

where α_i (i=1~24) are twenty-four undetermined coefficients; U_i, V_i and W_i (i=13~21) are the analytical general

solutions for quadratic displacements given by Equations (A20) to (A22); the first twelve columns of interpolation

matrix $\mathbf{P}$ are also displacement analytical general solutions satisfying all governing equations, as shown in Table 1.

The last three columns containing the cubic term RST are not the analytical solutions, but they can keep linear

independence between each two columns, and make the resulting stress components invariant for global

coordinate rotation.

Substitution of the Cartesian coordinates of eight corner nodes into Equation (24) yields

$$\hat{\mathbf{d}}\,\boldsymbol{\alpha} = \mathbf{q}^e, \tag{25}$$

where

$$\hat{\mathbf{d}} = \begin{bmatrix} \mathbf{P}(x_1, y_1, z_1) \\ \mathbf{P}(x_2, y_2, z_2) \\ \vdots \\ \mathbf{P}(x_8, y_8, z_8) \end{bmatrix}. \tag{26}$$

$$\mathbf{q}^e = [u_1 \quad v_1 \quad w_1 \quad \cdots \quad u_8 \quad v_8 \quad w_8]^{\mathrm{T}}, \tag{27}$$

in which u_i, v_i and w_i ($i =1\sim8$) are the nodal displacements along x-, y- and z- directions, respectively. Then, α_i

($i=1\sim24$) can be solved by

$$\boldsymbol{\alpha} = \hat{\mathbf{d}}^{-1}\mathbf{q}^e. \tag{28}$$

And the assumed displacement fields $\hat{\mathbf{u}}$ given by Equation (24) can be rewritten as

$$\hat{\mathbf{u}} = \left\{ \begin{array}{c} \hat{u} \\ \hat{v} \\ \hat{w} \end{array} \right\} = \mathbf{P}\boldsymbol{\alpha} = \mathbf{P}\hat{\mathbf{d}}^{-1}\mathbf{q}^e. \tag{29}$$

Then, the corresponding strains can be obtained by substituting equation (29) into (14)

$$\hat{\boldsymbol{\varepsilon}} = \begin{bmatrix} \hat{\varepsilon}_x & \hat{\varepsilon}_y & \hat{\varepsilon}_z & \hat{\gamma}_{xy} & \hat{\gamma}_{yz} & \hat{\gamma}_{zx} \end{bmatrix}^{\mathrm{T}} = \tilde{\mathbf{P}}\hat{\mathbf{d}}^{-1}\mathbf{q}^e = \hat{\mathbf{B}}\mathbf{q}^e, \tag{30}$$

where $\hat{\mathbf{B}} = \tilde{\mathbf{P}}\hat{\mathbf{d}}^{-1}$ is the strain matrix, and

$$\tilde{\mathbf{P}} = \begin{bmatrix} 0 & 0 & 0 & \dfrac{a_1}{J_0} & 0 & 0 & \dfrac{a_2}{J_0} & 0 & 0 & \dfrac{a_3}{J_0} & 0 & 0 & \varepsilon_{x13} & \cdots & \varepsilon_{x21} & u_a & 0 & 0 \\[6pt] 0 & 0 & 0 & 0 & \dfrac{b_1}{J_0} & 0 & 0 & \dfrac{b_2}{J_0} & 0 & 0 & \dfrac{b_3}{J_0} & 0 & \varepsilon_{y13} & \cdots & \varepsilon_{y21} & 0 & u_b & 0 \\[6pt] 0 & 0 & 0 & 0 & 0 & \dfrac{c_1}{J_0} & 0 & 0 & \dfrac{c_2}{J_0} & 0 & 0 & \dfrac{c_3}{J_0} & \varepsilon_{z13} & \cdots & \varepsilon_{z21} & 0 & 0 & u_c \\[6pt] 0 & 0 & 0 & \dfrac{b_1}{J_0} & \dfrac{a_1}{J_0} & 0 & \dfrac{b_2}{J_0} & \dfrac{a_2}{J_0} & 0 & \dfrac{b_3}{J_0} & \dfrac{a_3}{J_0} & 0 & \gamma_{xy13} & \cdots & \gamma_{xy21} & u_b & u_a & 0 \\[6pt] 0 & 0 & 0 & 0 & \dfrac{c_1}{J_0} & \dfrac{b_1}{J_0} & 0 & \dfrac{c_2}{J_0} & \dfrac{b_2}{J_0} & 0 & \dfrac{c_3}{J_0} & \dfrac{b_3}{J_0} & \gamma_{yz13} & \cdots & \gamma_{yz21} & 0 & u_c & u_b \\[6pt] 0 & 0 & 0 & \dfrac{c_1}{J_0} & 0 & \dfrac{a_1}{J_0} & \dfrac{c_2}{J_0} & 0 & \dfrac{a_2}{J_0} & \dfrac{c_3}{J_0} & 0 & \dfrac{a_3}{J_0} & \gamma_{xz13} & \cdots & \gamma_{xz21} & u_c & 0 & u_a \end{bmatrix}, \tag{31}$$

with

$$u_a = \frac{1}{J_0}(a_1 ST + a_2 RT + a_3 RS), \; u_b = \frac{1}{J_0}(b_1 ST + b_2 RT + b_3 RS), \; u_c = \frac{1}{J_0}(c_1 ST + c_2 RT + c_3 RS), \quad (32)$$

in which (ε_{xi}, ε_{yi}, ε_{zi}, γ_{xyi}, γ_{yzi}, γ_{zxi}) (i =13~21) are the nine sets of analytical solutions for linear strains given by Equations (A3) ,(A5), (A7), (A9), (A11), (A13), (A15), (A17) and (A19), respectively.

According to the constitutive relation Equation (13), the corresponding stresses can be solved

$$\hat{\boldsymbol{\sigma}} = \begin{Bmatrix} \hat{\sigma}_x \\ \hat{\sigma}_y \\ \hat{\sigma}_z \\ \hat{\tau}_{xy} \\ \hat{\tau}_{yz} \\ \hat{\tau}_{zx} \end{Bmatrix} = \mathbf{D}\hat{\boldsymbol{\varepsilon}} = \mathbf{D}\hat{\mathbf{B}}\mathbf{q}^e = \mathbf{D}\tilde{\mathbf{P}}\hat{\mathbf{d}}^{-1}\mathbf{q}^e, \quad (33)$$

where $\mathbf{D}$ is the elasticity matrix,

$$\mathbf{D} = \mathbf{C}^{-1}. \quad (34)$$

Substitution of Equations (16), (19) and (30) into (15) yields

$$\begin{aligned}
&\iiint_{V^e} \delta\tilde{\boldsymbol{\varepsilon}}^{\mathrm{T}}\hat{\boldsymbol{\sigma}}\mathrm{d}V - \iiint_{V^e} \delta\overline{\mathbf{u}}^{\mathrm{T}}\mathbf{b}\mathrm{d}V - \int_{\Gamma^e} \delta\overline{\mathbf{u}}^{\mathrm{T}}\mathbf{T}\mathrm{d}\Gamma - \delta\overline{\mathbf{u}}_c^{\mathrm{T}}\mathbf{f}_c \\
&= \iiint_{V^e} \delta\tilde{\boldsymbol{\varepsilon}}^{\mathrm{T}}\mathbf{D}\hat{\boldsymbol{\varepsilon}}\mathrm{d}V - \iiint_{V^e} \delta\overline{\mathbf{u}}^{\mathrm{T}}\mathbf{b}\mathrm{d}V - \int_{\Gamma^e} \delta\overline{\mathbf{u}}^{\mathrm{T}}\mathbf{T}\mathrm{d}\Gamma - \delta\overline{\mathbf{u}}_c^{\mathrm{T}}\mathbf{f}_c \\
&= (\delta\mathbf{q}^e)^{\mathrm{T}}(\iiint_{V^e} \overline{\mathbf{B}}^{\mathrm{T}}\mathbf{D}\hat{\mathbf{B}}\mathbf{q}^e\mathrm{d}V - \iiint_{V^e} \overline{\mathbf{N}}^{\mathrm{T}}\mathbf{b}\mathrm{d}V - \int_{\Gamma^e} \overline{\mathbf{N}}^{\mathrm{T}}\mathbf{T}\mathrm{d}\Gamma - \overline{\mathbf{N}}_c^{\mathrm{T}}\mathbf{f}_c), \\
&= (\delta\mathbf{q}^e)^{\mathrm{T}}(\mathbf{K}^e\mathbf{q}^e - \mathbf{F}^e) \\
&= 0
\end{aligned} \quad (35)$$

in which

$$\mathbf{K}^e = \iiint_{V^e} \overline{\mathbf{B}}^{\mathrm{T}}\mathbf{D}\hat{\mathbf{B}}\mathrm{d}V, \quad (36)$$

$$\mathbf{F}^e = \iiint_{V^e} \overline{\mathbf{N}}^{\mathrm{T}}\mathbf{b}\mathrm{d}V + \int_{\Gamma^e} \overline{\mathbf{N}}^{\mathrm{T}}\mathbf{T}\mathrm{d}\Gamma + \overline{\mathbf{N}}_c^{\mathrm{T}}\mathbf{f}_c. \quad (37)$$

Due to the arbitrariness of $\delta\mathbf{q}^e$ in Equation (35), the following finite element equation can be obtained

$$\mathbf{K}^e\mathbf{q}^e - \mathbf{F}^e = \mathbf{0}, \quad (38)$$

where $\mathbf{F}^e$ is the nodal equivalent load vector of the element; $\mathbf{K}^e$ is the element stiffness matrix, and it is an unsymmetric matrix. Substitution of Equations (20) and (33) into (36), the final element stiffness matrix can be

obtained

$$\mathbf{K}^e = \iiint_{V^e} \overline{\mathbf{B}}^\mathrm{T} \mathbf{D}\hat{\mathbf{B}} \mathrm{d}V = \int_{-1}^1 \int_{-1}^1 \int_{-1}^1 \frac{\overline{\mathbf{B}}^{*\mathrm{T}}}{|\mathbf{J}|} \mathbf{D}\hat{\mathbf{B}} |\mathbf{J}| \mathrm{d}\xi \mathrm{d}\eta \mathrm{d}\zeta$$

$$= \int_{-1}^1 \int_{-1}^1 \int_{-1}^1 \overline{\mathbf{B}}^{*\mathrm{T}} \mathbf{D}\hat{\mathbf{B}} \mathrm{d}\xi \mathrm{d}\eta \mathrm{d}\zeta = \int_{-1}^1 \int_{-1}^1 \int_{-1}^1 \overline{\mathbf{B}}^{*\mathrm{T}} \mathbf{D}\tilde{\mathbf{P}}\hat{\mathbf{d}}^{-1} \mathrm{d}\xi \mathrm{d}\eta \mathrm{d}\zeta$$

(39)

Because there is no Jacobian determinant existing in above expression, the resulting model will avoid troubles caused by ill-conditioned shape and be insensitive to mesh distortions. All above formulations can be expressed in terms of isoparametric coordinates ξ, η and ζ by using equations (4) and (23), and a 2×2×2 Gauss integration scheme is found to be enough for evaluating $\mathbf{K}^e$ given by Equation (39), although the 3×3×3 scheme is theoretically needed.

The equivalent nodal load vector $\mathbf{F}^e$ can be determined by the same procedure for the traditional 8-node tri-linear isoparametric element. And the stresses at any point can be directly calculated by substituting the isoparametric, or Cartesian coordinates of this point within an element into Equation (33).

The new element is denoted by US-ATFH8.

4. NUMERICAL EXAMPLES

In this section, some classical benchmark problems are employed to assess the performance of the new element US-ATFH8, and results obtained by other 8-node hexahedral elements listed in Table 2 are also given for comparisons.

4.1 Constant stress/strain patch test (Figure 3)

A unit cube, as shown in Figure 3, is divided by seven irregular hexahedral elements. Nodes 1 to 8 are the inner nodes, and their locations are also given in Figure 3. The displacement fields corresponding to the constant

strain are:

$$u = 10^{-3}(2x+y+z)/2, \quad v = 10^{-3}(x+2y+z)/2, \quad w = 10^{-3}(x+y+2z)/2. \quad (40)$$

And the corresponding stress solutions are:

$$\sigma_x = \sigma_y = \sigma_z = 2000, \qquad \tau_{xy} = \tau_{yz} = \tau_{zx} = 400. \quad (41)$$

The displacements of the boundary nodes are treated as the displacement boundary conditions. Exact results of the displacements and stresses at the inner nodes can be obtained by the new element US-ATFH8. Furthermore, the exact stresses at any point (by substituting the Cartesian coordinates into Equation (33)) can also be obtained. It can be concluded that the element US-ATFH8 can strictly pass the constant stress/strain patch test.

Elements Wilson_H8 [2] and HVCC8 series [27] in Table 2 cannot pass this patch test.

4.2 Cheung and Chen beam tests [17] (Figure 4)

This example was proposed by Cheung and Chen [17] for testing the performance of 8-node hexahedral elements. The geometric, material, and displacement boundary conditions are given in Figure 4. Twelve meshes divisions are designed to analyze this cantilever beam subjected to a pure bending moment M and a transverse shear force P at the free end, in which the x coordinates of nodes 1, 2, 3 and 4 in Meshes (2) to (10) are listed in Table 3. The normalized deflections at point A and the results of stresses at point B are given in Tables 4 and 5, respectively, and the results of deflections at points a_1, a_2, a_3 and a_4 in selected mesh divisions under loading P are also given in Table 6.

From Tables 4 and 5, it can be seen that exact displacements and stresses under pure bending state can be obtained by element TH8 (β =0.01 and 0.0001) [46] and the new element US-ATFH8, no matter how meshes are distorted, and no matter whether the four corner nodes of the interface are coplanar or not. Furthermore, it is worth mentioning that the new element US-ATFH8 can produce exact pure bending solutions in all directions when various distorted meshes are used. For the linear bending case, the new element US-ATFH8 can also present

relatively good and stable solutions in all mesh cases. But the results obtained by element TH8 deeply depend on the adjustable factor β and are not stable. Especially, when β=0.0001, even wrong solutions will appear in some cases (see displacement result for load P using Mesh (12) in Table 4). This problem is more clear in Table 6, many incorrect results for deflections at four different end points of the beam obtained by element TH8 appear when β=0.0001, and the results obtained by TH8 (β=0.01) are not stable in some occasions.

4.3 Rotational frame dependence test on a cantilever beam with fully fixed end (Figure 5)

Since the trial functions for displacements $\hat{\mathbf{u}}$ given in Equation (24) may be not completed in the global Cartesian coordinates, rotational frame dependence test should be performed for the new element US-ATFH8.

The geometric and displacement boundary conditions of a cantilever beam divided by two distorted elements are given in Figure 5. The Young's modulus E=100.0, and the Poisson ratio μ=0.3. Let the Cartesian coordinate system xyz rotate counterclockwise from α_1=0° to 90° in steps of 10° around z-axis, and then rotate counterclockwise α_2=40° around y-axis, the displacements at point A are solved at each step. The magnitude of displacement $\sqrt{u^2+v^2+w^2}$ at point A is monitored to study the rotational frame-dependent behavior. The results obtained by the new element US-ATFH8 are given in Table 7. The magnitude of displacements based on an 'overkill' solution is used as a reference solution, which is obtained by using 50000 20-node hexahedral isoparametric elements of Abaqus [1]. It can be seen that the present model US-ATFH8 provides the invariance for the coordinate rotation.

4.4 Bending problems for skew beam, curving beam and twisted beam

4.4.1 Cook's skew beam problem (Figure 6)

This example shown in Figure 6 was proposed by Cook [56] to test the convergence of elements. A skew

cantilever is subjected to a shear uniformly distributed load at the free edge. The geometric, material and

displacement boundary conditions are given in Figure 6. The results of vertical deflection at point C, the

maximum principal stress at point A and the minimum principal stress at point B are all listed in Table 8. Those

results obtained by the models that can pass the constant strain/stress patch test are also given for comparison. It

can be seen that the present element US-ATFH8 exhibits good convergence.

4.4.2 Thin curved beam (Figure 7)

A thin curved beam with fully fixed end is shown in Figure 7. The inner radius R_i, thickness h and width t of

the beam are 4.12, 0.2 and 0.1, respectively. The Young's modulus $E=1.0\times10^7$, and the Poisson ratio $\mu=0.3$. Two

load cases are considered: in-plane shear P_1 and out-of-plane shear P_2. The results of the deflection at point A are

listed in Tables 9 and 10, respectively. Again, the new element US-ATFH8 performs well for this test.

4.4.3 Twisted beam problem (Figure 8)

This example was proposed by MacNeal and Harder [57] to test the effect of warping. As shown in Figure 8, a

cantilever beam is twisted 90º from root to tip. This twisted beam is fixed at the root, and subjected to unit

in-plane and out-of-plane forces at the tip. The length, width and thickness are 12, 1.1 and 0.32, respectively. The

Young's modulus $E=2.9\times10^7$, and the Poisson ratio $\mu=0.22$. Different meshes used for this example are also given

in Figure 8, in which meshes (a), (b), (c) and (d) are distorted meshes newly designed by cutting the beam with

different planes. And most of these cutting planes are parallel to new plane *xy* after *x*-axis rotates 45º or -45º

around *y*-axis. The normalized solutions at tip point A are listed in Table 11 and 12. It can be seen that the new

element US-ATFH8 can produce better results, even when the severely distorted meshes are used.

4.5 Nearly incompressible problems (Figure 9)

A thick-walled cylinder is subjected to a uniformly distributed internal pressure $p=1$. This example, proposed by MacNeal [57], is used to test volume locking problem when the Poisson's ratio is very close to 0.5. As shown in Figure 9, due to symmetry, only a quarter of the cylinder with unit thickness is considered. The nodal displacements along thickness direction are all constrained. The exact solution of the radial displacement u_r is same as that for the plane strain state, and given by [57]

$$u_r = \frac{(1+\mu)pR_1^2}{E(R_2^2 - R_1^2)}\left[R_2^2/r + (1-2\mu)r\right], \tag{42}$$

where R_1 is the inner radius, R_2 is the outer radius. In this example, let $R_1=3$, $R_2=9$. When the Poisson's ratio is $\mu = 0.49, 0.499, 0.4999$, the corresponding radial displacement u_r at $r=R_1$ are 5.0399×10^{-3}, 5.0602×10^{-3}, 5.0623×10^{-3}, respectively.

The normalized results of the radial displacement u_r at $r=R_1$ are given in Table 13. It can be seen that the standard 8-node tri-linear isoparametric element suffers from volumetric locking problem, while other improved models can give good results. Although the solutions obtained by element US-ATFH8 are not the best answers, it is clearly shown that the new element is free of the volumetric locking.

5. CONCLUSIONS

After successful development of plane 4-node, 8-DOF quadrilateral element US-ATFQ4 [45] which can break through the limitation defined by MacNeal [6, 7], a new 3D 8-node hexahedral element US-ATFH8 is constructed by employing the unsymmetric element method, the analytical trial function method and the oblique coordinate method. This new 3D low-order element, which can be treated as an extension from the plane element US-ATFQ4, possesses following advantages superior to most existing 8-node hexahedral element models:

(i)   Its formulations contain no adjustable factor, and can be used for both isotropic and anisotropic cases;

(ii)   It can strictly pass both the first-order (constant stress/strain) patch test and the second-order patch test for pure bending (free of trapezoidal locking), which cannot be achieved by most other existing finite element models;

(iii) It is free of volume locking, and provides the invariance for coordinate rotation;

(iv) It is insensitive to various mesh distortions, and can produce stable and better solutions for higher-order problems (the orders of the displacement fields are higher than first- and second-order).

The appearance of above new low-order elements with high accuracy and distortion resistance may open a way for establishing new finite element system which can relax the requirements for hexahedron mesh generation. This point may have great significance for further development of the finite element method. Although the element stiffness matrix is unsymmetric, it is not a serious issue in most of the problems in structural analyses: many solvers can handle this situation easily [1, 58].

Of course, before this new model can be really applied in practical engineering, many further technique problems must be solved. Whether the present method can be extended to the applications of shell and nonlinear problems is still a valuable and challenging research topic that should be paid attention to. Some related developments will be reported in near future.

APPENDIX A: NINE SETS OF ANALYTICAL GENERAL SOLUTIONS FOR GLOBAL LINEAR STRESSES, STRAINS AND QUADRATIC DISPLACEMENTS IN TERMS OF R, S AND T

Let

$$h_1 = \bar{b}_2\bar{c}_3 + \bar{b}_3\bar{c}_2, \qquad h_2 = \bar{a}_2\bar{c}_3 + \bar{a}_3\bar{c}_2, \qquad h_3 = \bar{a}_2\bar{b}_3 + \bar{a}_3\bar{b}_2$$

$$h_4 = \bar{b}_1\bar{c}_3 + \bar{b}_3\bar{c}_1, \qquad h_5 = \bar{a}_1\bar{c}_3 + \bar{a}_3\bar{c}_1, \qquad h_6 = \bar{a}_1\bar{b}_3 + \bar{a}_3\bar{b}_1 \ . \qquad \text{(A1)}$$

$$h_7 = \bar{b}_1\bar{c}_2 + \bar{b}_2\bar{c}_1, \qquad h_8 = \bar{a}_1\bar{c}_2 + \bar{a}_2\bar{c}_1, \qquad h_9 = \bar{a}_1\bar{b}_2 + \bar{a}_2\bar{b}_1$$

Then, from Equations (11) to (14), the resulting solutions for global linear stresses, strains and quadratic displacements can be written as follows.

1. Nine sets of analytical general solutions for global linear stresses and strains in terms of R, S and T

(1) The 13th set of solutions for global stresses and strains

Stresses:

$$\sigma_{x13} = \bar{a}_2^2 R, \quad \sigma_{y13} = \bar{b}_2^2 R, \quad \sigma_{z13} = \bar{c}_2^2 R, \quad \tau_{xy13} = \bar{a}_2\bar{b}_2 R, \quad \tau_{yz13} = \bar{b}_2\bar{c}_2 R, \quad \tau_{zx13} = \bar{a}_2\bar{c}_2 R ; \quad \text{(A2)}$$

Strains:

for isotropic case

$$\begin{cases} \varepsilon_{x13} = \dfrac{1}{E}(\bar{a}_2^2 - \mu\bar{b}_2^2 - \mu\bar{c}_2^2)R = A_{x13}R, \quad \varepsilon_{y13} = \dfrac{1}{E}(\bar{b}_2^2 - \mu\bar{a}_2^2 - \mu\bar{c}_2^2)R = A_{y13}R \\[2mm] \varepsilon_{z13} = \dfrac{1}{E}(\bar{c}_2^2 - \mu\bar{a}_2^2 - \mu\bar{b}_2^2)R = A_{z13}R, \quad \gamma_{xy13} = \dfrac{2(1+\mu)}{E}\bar{a}_2\bar{b}_2 R = A_{xy13}R \\[2mm] \gamma_{yz13} = \dfrac{2(1+\mu)}{E}\bar{b}_2\bar{c}_2 R = A_{yz13}R, \qquad\qquad \gamma_{zx13} = \dfrac{2(1+\mu)}{E}\bar{a}_2\bar{c}_2 R = A_{zx13}R \end{cases} , \quad \text{(A3a)}$$

for anisotropic case

$$\begin{cases} \varepsilon_{x13} = (\bar{a}_2^2 C_{11} + \bar{b}_2^2 C_{12} + \bar{c}_2^2 C_{13} + \bar{a}_2\bar{b}_2 C_{14} + \bar{b}_2\bar{c}_2 C_{15} + \bar{a}_2\bar{c}_2 C_{16})R = A_{x13}R \\ \varepsilon_{y13} = (\bar{a}_2^2 C_{21} + \bar{b}_2^2 C_{22} + \bar{c}_2^2 C_{23} + \bar{a}_2\bar{b}_2 C_{24} + \bar{b}_2\bar{c}_2 C_{25} + \bar{a}_2\bar{c}_2 C_{26})R = A_{y13}R \\ \varepsilon_{z13} = (\bar{a}_2^2 C_{31} + \bar{b}_2^2 C_{32} + \bar{c}_2^2 C_{33} + \bar{a}_2\bar{b}_2 C_{34} + \bar{b}_2\bar{c}_2 C_{35} + \bar{a}_2\bar{c}_2 C_{36})R = A_{z13}R \\ \gamma_{xy13} = (\bar{a}_2^2 C_{41} + \bar{b}_2^2 C_{42} + \bar{c}_2^2 C_{43} + \bar{a}_2\bar{b}_2 C_{44} + \bar{b}_2\bar{c}_2 C_{45} + \bar{a}_2\bar{c}_2 C_{46})R = A_{xy13}R \\ \gamma_{yz13} = (\bar{a}_2^2 C_{51} + \bar{b}_2^2 C_{52} + \bar{c}_2^2 C_{53} + \bar{a}_2\bar{b}_2 C_{54} + \bar{b}_2\bar{c}_2 C_{55} + \bar{a}_2\bar{c}_2 C_{56})R = A_{yz13}R \\ \gamma_{zx13} = (\bar{a}_2^2 C_{61} + \bar{b}_2^2 C_{62} + \bar{c}_2^2 C_{63} + \bar{a}_2\bar{b}_2 C_{64} + \bar{b}_2\bar{c}_2 C_{65} + \bar{a}_2\bar{c}_2 C_{66})R = A_{zx13}R \end{cases} . \quad \text{(A3b)}$$

(2) The 14th set of solutions for global stresses and strains

Stresses:

$$\sigma_{x14} = \bar{a}_3^2 R, \quad \sigma_{y14} = \bar{b}_3^2 R, \quad \sigma_{z14} = \bar{c}_3^2 R, \quad \tau_{xy14} = \bar{a}_3\bar{b}_3 R, \quad \tau_{yz14} = \bar{b}_3\bar{c}_3 R, \quad \tau_{zx14} = \bar{a}_3\bar{c}_3 R ; \quad \text{(A4)}$$

Strains:

for isotropic case

$$
\begin{cases}
\varepsilon_{x14} = \dfrac{1}{E}(\bar{a}_3^2 - \mu\bar{b}_3^2 - \mu\bar{c}_3^2)R = A_{x14}R, \quad \varepsilon_{y14} = \dfrac{1}{E}(\bar{b}_3^2 - \mu\bar{a}_3^2 - \mu\bar{c}_3^2)R = A_{y14}R \\[2mm]
\varepsilon_{z14} = \dfrac{1}{E}(\bar{c}_3^2 - \mu\bar{a}_3^2 - \mu\bar{b}_3^2)R = A_{z14}R, \quad \gamma_{xy14} = \dfrac{2(1+\mu)}{E}\bar{a}_3\bar{b}_3 R = A_{xy14}R \\[2mm]
\gamma_{yz14} = \dfrac{2(1+\mu)}{E}\bar{b}_3\bar{c}_3 R = A_{yz14}R, \quad\quad\quad \gamma_{zx14} = \dfrac{2(1+\mu)}{E}\bar{a}_3\bar{c}_3 R = A_{zx14}R
\end{cases}
\quad , \quad \text{(A5a)}
$$

for anisotropic case

$$
\begin{cases}
\varepsilon_{x14} = (\bar{a}_3^2 C_{11} + \bar{b}_3^2 C_{12} + \bar{c}_3^2 C_{13} + \bar{a}_3\bar{b}_3 C_{14} + \bar{b}_3\bar{c}_3 C_{15} + \bar{a}_3\bar{c}_3 C_{16})R = A_{x14}R \\
\varepsilon_{y14} = (\bar{a}_3^2 C_{21} + \bar{b}_3^2 C_{22} + \bar{c}_3^2 C_{23} + \bar{a}_3\bar{b}_3 C_{24} + \bar{b}_3\bar{c}_3 C_{25} + \bar{a}_3\bar{c}_3 C_{26})R = A_{y14}R \\
\varepsilon_{z14} = (\bar{a}_3^2 C_{31} + \bar{b}_3^2 C_{32} + \bar{c}_3^2 C_{33} + \bar{a}_3\bar{b}_3 C_{34} + \bar{b}_3\bar{c}_3 C_{35} + \bar{a}_3\bar{c}_3 C_{36})R = A_{z14}R \\
\gamma_{xy14} = (\bar{a}_3^2 C_{41} + \bar{b}_3^2 C_{42} + \bar{c}_3^2 C_{43} + \bar{a}_3\bar{b}_3 C_{44} + \bar{b}_3\bar{c}_3 C_{45} + \bar{a}_3\bar{c}_3 C_{46})R = A_{xy14}R \\
\gamma_{yz14} = (\bar{a}_3^2 C_{51} + \bar{b}_3^2 C_{52} + \bar{c}_3^2 C_{53} + \bar{a}_3\bar{b}_3 C_{54} + \bar{b}_3\bar{c}_3 C_{55} + \bar{a}_3\bar{c}_3 C_{56})R = A_{yz14}R \\
\gamma_{zx14} = (\bar{a}_3^2 C_{61} + \bar{b}_3^2 C_{62} + \bar{c}_3^2 C_{63} + \bar{a}_3\bar{b}_3 C_{64} + \bar{b}_3\bar{c}_3 C_{65} + \bar{a}_3\bar{c}_3 C_{66})R = A_{zx14}R
\end{cases}
\quad \text{(A5b)}
$$

(3) The 15th set of solutions for global stresses and strains

Stresses:

$$
\sigma_{x15} = 2\bar{a}_2\bar{a}_3 R, \quad \sigma_{y15} = 2\bar{b}_2\bar{b}_3 R, \quad \sigma_{z15} = 2\bar{c}_2\bar{c}_3 R, \quad \tau_{xy15} = h_3 R, \quad \tau_{yz15} = h_1 R, \quad \tau_{zx15} = h_2 R ; \quad \text{(A6)}
$$

Strains:

for isotropic case

$$
\begin{cases}
\varepsilon_{x15} = \dfrac{2}{E}(\bar{a}_2\bar{a}_3 - \mu\bar{b}_2\bar{b}_3 - \mu\bar{c}_2\bar{c}_3)R = A_{x15}R, \quad \varepsilon_{y15} = \dfrac{2}{E}(\bar{b}_2\bar{b}_3 - \mu\bar{a}_2\bar{a}_3 - \mu\bar{c}_2\bar{c}_3)R = A_{y15}R \\[2mm]
\varepsilon_{z15} = \dfrac{2}{E}(\bar{c}_2\bar{c}_3 - \mu\bar{a}_2\bar{a}_3 - \mu\bar{b}_2\bar{b}_3)R = A_{z15}R, \quad \gamma_{xy15} = \dfrac{2(1+\mu)}{E}(\bar{a}_2\bar{b}_3 + \bar{a}_3\bar{b}_2)R = A_{xy15}R \\[2mm]
\gamma_{yz15} = \dfrac{2(1+\mu)}{E}(\bar{b}_2\bar{c}_3 + \bar{b}_3\bar{c}_2)R = A_{yz15}R, \quad \gamma_{zx15} = \dfrac{2(1+\mu)}{E}(\bar{a}_2\bar{c}_3 + \bar{a}_3\bar{c}_2)R = A_{zx15}R
\end{cases}
\quad , \text{(A7a)}
$$

for anisotropic case

$$\begin{cases} \varepsilon_{x15} = (2\bar{a}_2\bar{a}_3 C_{11} + 2\bar{b}_2\bar{b}_3 C_{12} + 2\bar{c}_2\bar{c}_3 C_{13} + h_3 C_{14} + h_1 C_{15} + h_2 C_{16})R = A_{x15}R \\ \varepsilon_{y15} = (2\bar{a}_2\bar{a}_3 C_{21} + 2\bar{b}_2\bar{b}_3 C_{22} + 2\bar{c}_2\bar{c}_3 C_{23} + h_3 C_{24} + h_1 C_{25} + h_2 C_{26})R = A_{y15}R \\ \varepsilon_{z15} = (2\bar{a}_2\bar{a}_3 C_{31} + 2\bar{b}_2\bar{b}_3 C_{32} + 2\bar{c}_2\bar{c}_3 C_{33} + h_3 C_{34} + h_1 C_{35} + h_2 C_{36})R = A_{z15}R \\ \gamma_{xy15} = (2\bar{a}_2\bar{a}_3 C_{41} + 2\bar{b}_2\bar{b}_3 C_{42} + 2\bar{c}_2\bar{c}_3 C_{43} + h_3 C_{44} + h_1 C_{45} + h_2 C_{46})R = A_{xy15}R \\ \gamma_{yz15} = (2\bar{a}_2\bar{a}_3 C_{51} + 2\bar{b}_2\bar{b}_3 C_{52} + 2\bar{c}_2\bar{c}_3 C_{53} + h_3 C_{54} + h_1 C_{55} + h_2 C_{56})R = A_{yz15}R \\ \gamma_{zx15} = (2\bar{a}_2\bar{a}_3 C_{61} + 2\bar{b}_2\bar{b}_3 C_{62} + 2\bar{c}_2\bar{c}_3 C_{63} + h_3 C_{64} + h_1 C_{65} + h_2 C_{66})R = A_{zx15}R \end{cases} \quad \text{(A7b)}$$

(4) The 16th set of solutions for global stresses and strains

Stresses:

$$\sigma_{x16} = \bar{a}_1^2 S, \quad \sigma_{y16} = \bar{b}_1^2 S, \quad \sigma_{z16} = \bar{c}_1^2 S, \quad \tau_{xy16} = \bar{a}_1\bar{b}_1 S, \quad \tau_{yz16} = \bar{b}_1\bar{c}_1 S, \quad \tau_{zx16} = \bar{a}_1\bar{c}_1 S ; \quad \text{(A8)}$$

Strains:

for isotropic case

$$\begin{cases} \varepsilon_{x16} = \dfrac{1}{E}(\bar{a}_1^2 - \mu\bar{b}_1^2 - \mu\bar{c}_1^2)S = A_{x16}S, \quad \varepsilon_{y16} = \dfrac{1}{E}(\bar{b}_1^2 - \mu\bar{a}_1^2 - \mu\bar{c}_1^2)S = A_{y16}S \\ \varepsilon_{z16} = \dfrac{1}{E}(\bar{c}_1^2 - \mu\bar{a}_1^2 - \mu\bar{b}_1^2)S = A_{z16}S, \quad \gamma_{xy16} = \dfrac{2(1+\mu)}{E}\bar{a}_1\bar{b}_1 S = A_{xy16}S \\ \gamma_{yz16} = \dfrac{2(1+\mu)}{E}\bar{b}_1\bar{c}_1 S = A_{yz16}S, \quad\quad\quad \gamma_{zx16} = \dfrac{2(1+\mu)}{E}\bar{a}_1\bar{c}_1 S = A_{zx16}S \end{cases} \quad \text{, (A9a)}$$

for anisotropic case

$$\begin{cases} \varepsilon_{x16} = (\bar{a}_1^2 C_{11} + \bar{b}_1^2 C_{12} + \bar{c}_1^2 C_{13} + \bar{a}_1\bar{b}_1 C_{14} + \bar{b}_1\bar{c}_1 C_{15} + \bar{a}_1\bar{c}_1 C_{16})S = A_{x16}S \\ \varepsilon_{y16} = (\bar{a}_1^2 C_{21} + \bar{b}_1^2 C_{22} + \bar{c}_1^2 C_{23} + \bar{a}_1\bar{b}_1 C_{24} + \bar{b}_1\bar{c}_1 C_{25} + \bar{a}_1\bar{c}_1 C_{26})S = A_{y16}S \\ \varepsilon_{z16} = (\bar{a}_1^2 C_{31} + \bar{b}_1^2 C_{32} + \bar{c}_1^2 C_{33} + \bar{a}_1\bar{b}_1 C_{34} + \bar{b}_1\bar{c}_1 C_{35} + \bar{a}_1\bar{c}_1 C_{36})S = A_{z16}S \\ \gamma_{xy16} = (\bar{a}_1^2 C_{41} + \bar{b}_1^2 C_{42} + \bar{c}_1^2 C_{43} + \bar{a}_1\bar{b} C_{44} + \bar{b}_1\bar{c}_1 C_{45} + \bar{a}_1\bar{c}_1 C_{46})S = A_{xy16}S \\ \gamma_{yz16} = (\bar{a}_1^2 C_{51} + \bar{b}_1^2 C_{52} + \bar{c}_1^2 C_{53} + \bar{a}_1\bar{b}_1 C_{54} + \bar{b}_1\bar{c}_1 C_{55} + \bar{a}_1\bar{c}_1 C_{56})S = A_{yz16}S \\ \gamma_{zx16} = (\bar{a}_1^2 C_{61} + \bar{b}_1^2 C_{62} + \bar{c}_1^2 C_{63} + \bar{a}_1\bar{b}_1 C_{64} + \bar{b}_1\bar{c}_1 C_{65} + \bar{a}_1\bar{c}_1 C_{66})S = A_{zx16}S \end{cases} \quad \text{(A9b)}$$

(5) The 17th set of solutions for global stresses and strains

Stresses:

$$\sigma_{x17} = \bar{a}_3^2 S, \quad \sigma_{y17} = \bar{b}_3^2 S, \quad \sigma_{z17} = \bar{c}_3^2 S, \quad \tau_{xy17} = \bar{a}_3\bar{b}_3 S, \quad \tau_{yz17} = \bar{b}_3\bar{c}_3 S, \quad \tau_{zx17} = \bar{a}_3\bar{c}_3 S ; \quad \text{(A10)}$$

Strains:

for isotropic case

$$
\begin{cases}
\varepsilon_{x17} = \dfrac{1}{E}(\bar{a}_3^2 - \mu\bar{b}_3^2 - \mu\bar{c}_3^2)S = A_{x17}S, \quad & \varepsilon_{y17} = \dfrac{1}{E}(\bar{b}_3^2 - \mu\bar{a}_3^2 - \mu\bar{c}_3^2)S = A_{y17}S \\[2mm]
\varepsilon_{z17} = \dfrac{1}{E}(\bar{c}_3^2 - \mu\bar{a}_3^2 - \mu\bar{b}_3^2)S = A_{z17}S, \quad & \gamma_{xy17} = \dfrac{2(1+\mu)}{E}\bar{a}_3\bar{b}_3 S = A_{xy17}S \\[2mm]
\gamma_{yz17} = \dfrac{2(1+\mu)}{E}\bar{b}_3\bar{c}_3 S = A_{yz17}S, \quad & \gamma_{zx17} = \dfrac{2(1+\mu)}{E}\bar{a}_3\bar{c}_3 S = A_{zx17}S
\end{cases}
\quad , \quad \text{(A11a)}
$$

for anisotropic case

$$
\begin{cases}
\varepsilon_{x17} = (\bar{a}_3^2 C_{11} + \bar{b}_3^2 C_{12} + \bar{c}_3^2 C_{13} + \bar{a}_3\bar{b}_3 C_{14} + \bar{b}_3\bar{c}_3 C_{15} + \bar{a}_3\bar{c}_3 C_{16})S = A_{x17}S \\
\varepsilon_{y17} = (\bar{a}_3^2 C_{21} + \bar{b}_3^2 C_{22} + \bar{c}_3^2 C_{23} + \bar{a}_3\bar{b}_3 C_{24} + \bar{b}_3\bar{c}_3 C_{25} + \bar{a}_3\bar{c}_3 C_{26})S = A_{y17}S \\
\varepsilon_{z17} = (\bar{a}_3^2 C_{31} + \bar{b}_3^2 C_{32} + \bar{c}_3^2 C_{33} + \bar{a}_3\bar{b}_3 C_{34} + \bar{b}_3\bar{c}_3 C_{35} + \bar{a}_3\bar{c}_3 C_{36})S = A_{z17}S \\
\gamma_{xy17} = (\bar{a}_3^2 C_{41} + \bar{b}_3^2 C_{42} + \bar{c}_3^2 C_{43} + \bar{a}_3\bar{b}_3 C_{44} + \bar{b}_3\bar{c}_3 C_{45} + \bar{a}_3\bar{c}_3 C_{46})S = A_{xy17}S \\
\gamma_{yz17} = (\bar{a}_3^2 C_{51} + \bar{b}_3^2 C_{52} + \bar{c}_3^2 C_{53} + \bar{a}_3\bar{b}_3 C_{54} + \bar{b}_3\bar{c}_3 C_{55} + \bar{a}_3\bar{c}_3 C_{56})S = A_{yz17}S \\
\gamma_{zx17} = (\bar{a}_3^2 C_{61} + \bar{b}_3^2 C_{62} + \bar{c}_3^2 C_{63} + \bar{a}_3\bar{b}_3 C_{64} + \bar{b}_3\bar{c}_3 C_{65} + \bar{a}_3\bar{c}_3 C_{66})S = A_{zx17}S
\end{cases}
\quad \text{(A11b)}
$$

(6) The 18th set of solutions for global stresses and strains

Stresses:

$$
\sigma_{x18} = 2\bar{a}_1\bar{a}_3 S, \quad \sigma_{y18} = 2\bar{b}_1\bar{b}_3 S, \quad \sigma_{z18} = 2\bar{c}_1\bar{c}_3 S, \quad \tau_{xy18} = h_6 S, \quad \tau_{yz18} = h_4 S, \quad \tau_{zx18} = h_5 S ; \quad \text{(A12)}
$$

Strains:

for isotropic case

$$
\begin{cases}
\varepsilon_{x18} = \dfrac{2}{E}(\bar{a}_1\bar{a}_3 - \mu\bar{b}_1\bar{b}_3 - \mu\bar{c}_1\bar{c}_3)S = A_{x18}S, \quad & \varepsilon_{y18} = \dfrac{2}{E}(\bar{b}_1\bar{b}_3 - \mu\bar{a}_1\bar{a}_3 - \mu\bar{c}_1\bar{c}_3)S = A_{y18}S \\[2mm]
\varepsilon_{z18} = \dfrac{2}{E}(\bar{c}_1\bar{c}_3 - \mu\bar{a}_1\bar{a}_3 - \mu\bar{b}_1\bar{b}_3)S = A_{z18}S, \quad & \gamma_{xy18} = \dfrac{2(1+\mu)}{E}(\bar{a}_1\bar{b}_3 + \bar{a}_3\bar{b}_1)S = A_{xy18}S \\[2mm]
\gamma_{yz18} = \dfrac{2(1+\mu)}{E}(\bar{b}_1\bar{c}_3 + \bar{b}_3\bar{c}_1)S = A_{yz18}S, \quad & \gamma_{zx18} = \dfrac{2(1+\mu)}{E}(\bar{a}_1\bar{c}_3 + \bar{a}_3\bar{c}_1)S = A_{zx18}S
\end{cases}
\quad , \quad \text{(A13a)}
$$

for anisotropic case

$$
\begin{cases}
\varepsilon_{x18} = (2\bar{a}_1\bar{a}_3 C_{11} + 2\bar{b}_1\bar{b}_3 C_{12} + 2\bar{c}_1\bar{c}_3 C_{13} + h_6 C_{14} + h_4 C_{15} + h_5 C_{16})S = A_{x18}S \\
\varepsilon_{y18} = (2\bar{a}_1\bar{a}_3 C_{21} + 2\bar{b}_1\bar{b}_3 C_{22} + 2\bar{c}_1\bar{c}_3 C_{23} + h_6 C_{24} + h_4 C_{25} + h_5 C_{26})S = A_{y18}S \\
\varepsilon_{z18} = (2\bar{a}_1\bar{a}_3 C_{31} + 2\bar{b}_1\bar{b}_3 C_{32} + 2\bar{c}_1\bar{c}_3 C_{33} + h_6 C_{34} + h_4 C_{35} + h_5 C_{36})S = A_{z18}S \\
\gamma_{xy18} = (2\bar{a}_1\bar{a}_3 C_{41} + 2\bar{b}_1\bar{b}_3 C_{42} + 2\bar{c}_1\bar{c}_3 C_{43} + h_6 C_{44} + h_4 C_{45} + h_5 C_{46})S = A_{xy18}S \\
\gamma_{yz18} = (2\bar{a}_1\bar{a}_3 C_{51} + 2\bar{b}_1\bar{b}_3 C_{52} + 2\bar{c}_1\bar{c}_3 C_{53} + h_6 C_{54} + h_4 C_{55} + h_5 C_{56})S = A_{yz18}S \\
\gamma_{zx18} = (2\bar{a}_1\bar{a}_3 C_{61} + 2\bar{b}_1\bar{b}_3 C_{62} + 2\bar{c}_1\bar{c}_3 C_{63} + h_6 C_{64} + h_4 C_{65} + h_5 C_{66})S = A_{zx18}S
\end{cases}
\tag{A13b}
$$

(7) The 19th set of solutions for global stresses and strains

Stresses:

$$
\sigma_{x19} = \bar{a}_1^2 T, \quad \sigma_{y19} = \bar{b}_1^2 T, \quad \sigma_{z19} = \bar{c}_1^2 T, \quad \tau_{xy19} = \bar{a}_1\bar{b}_1 T, \quad \tau_{yz19} = \bar{b}_1\bar{c}_1 T, \quad \tau_{zx19} = \bar{a}_1\bar{c}_1 T ; \quad \text{(A14)}
$$

Strains:

for isotropic case

$$
\begin{cases}
\varepsilon_{x19} = \dfrac{1}{E}(\bar{a}_1^2 - \mu\bar{b}_1^2 - \mu\bar{c}_1^2)T = A_{x19}T, \qquad \varepsilon_{y19} = \dfrac{1}{E}(\bar{b}_1^2 - \mu\bar{a}_1^2 - \mu\bar{c}_1^2)T = A_{y19}T \\[2mm]
\varepsilon_{z19} = \dfrac{1}{E}(\bar{c}_1^2 - \mu\bar{a}_1^2 - \mu\bar{b}_1^2)T = A_{z19}T, \qquad \gamma_{xy19} = \dfrac{2(1+\mu)}{E}\bar{a}_1\bar{b}_1 T = A_{xy19}T \\[2mm]
\gamma_{yz19} = \dfrac{2(1+\mu)}{E}\bar{b}_1\bar{c}_1 T = A_{yz19}T, \qquad\qquad \gamma_{zx19} = \dfrac{2(1+\mu)}{E}\bar{a}_1\bar{c}_1 T = A_{zx19}T
\end{cases}
, \quad \text{(A15a)}
$$

for anisotropic case

$$
\begin{cases}
\varepsilon_{x19} = (\bar{a}_1^2 C_{11} + \bar{b}_1^2 C_{12} + \bar{c}_1^2 C_{13} + \bar{a}_1\bar{b}_1 C_{14} + \bar{b}_1\bar{c}_1 C_{15} + \bar{a}_1\bar{c}_1 C_{16})T = A_{x19}T \\
\varepsilon_{y19} = (\bar{a}_1^2 C_{21} + \bar{b}_1^2 C_{22} + \bar{c}_1^2 C_{23} + \bar{a}_1\bar{b}_1 C_{24} + \bar{b}_1\bar{c}_1 C_{25} + \bar{a}_1\bar{c}_1 C_{26})T = A_{y19}T \\
\varepsilon_{z19} = (\bar{a}_1^2 C_{31} + \bar{b}_1^2 C_{32} + \bar{c}_1^2 C_{33} + \bar{a}_1\bar{b}_1 C_{34} + \bar{b}_1\bar{c}_1 C_{35} + \bar{a}_1\bar{c}_1 C_{36})T = A_{z19}T \\
\gamma_{xy19} = (\bar{a}_1^2 C_{41} + \bar{b}_1^2 C_{42} + \bar{c}_1^2 C_{43} + \bar{a}_1\bar{b} C_{44} + \bar{b}_1\bar{c}_1 C_{45} + \bar{a}_1\bar{c}_1 C_{46})T = A_{xy19}T \\
\gamma_{yz19} = (\bar{a}_1^2 C_{51} + \bar{b}_1^2 C_{52} + \bar{c}_1^2 C_{53} + \bar{a}_1\bar{b}_1 C_{54} + \bar{b}_1\bar{c}_1 C_{55} + \bar{a}_1\bar{c}_1 C_{56})T = A_{yz19}T \\
\gamma_{zx19} = (\bar{a}_1^2 C_{61} + \bar{b}_1^2 C_{62} + \bar{c}_1^2 C_{63} + \bar{a}_1\bar{b}_1 C_{64} + \bar{b}_1\bar{c}_1 C_{65} + \bar{a}_1\bar{c}_1 C_{66})T = A_{zx19}T
\end{cases}
\tag{A15b}
$$

(8) The 20th set of solutions for global stresses and strains

Stresses:

$$
\sigma_{x20} = \bar{a}_2^2 T, \quad \sigma_{y20} = \bar{b}_2^2 T, \quad \sigma_{z20} = \bar{c}_2^2 T, \quad \tau_{xy20} = \bar{a}_2\bar{b}_2 T, \quad \tau_{yz20} = \bar{b}_2\bar{c}_2 T, \quad \tau_{zx20} = \bar{a}_2\bar{c}_2 T ; \quad \text{(A16)}
$$

Strains:

for isotropic case

$$
\begin{cases}
\varepsilon_{x20} = \dfrac{1}{E}(\bar{a}_2^2 - \mu\bar{b}_2^2 - \mu\bar{c}_2^2)T = A_{x20}T, \quad & \varepsilon_{y20} = \dfrac{1}{E}(\bar{b}_2^2 - \mu\bar{a}_2^2 - \mu\bar{c}_2^2)T = A_{y20}T \\[2mm]
\varepsilon_{z20} = \dfrac{1}{E}(\bar{c}_2^2 - \mu\bar{a}_2^2 - \mu\bar{b}_2^2)T = A_{z20}T, \quad & \gamma_{xy20} = \dfrac{2(1+\mu)}{E}\bar{a}_2\bar{b}_2 T = A_{xy20}T \\[2mm]
\gamma_{yz20} = \dfrac{2(1+\mu)}{E}\bar{b}_2\bar{c}_2 T = A_{yz20}T, \quad & \gamma_{zx20} = \dfrac{2(1+\mu)}{E}\bar{a}_2\bar{c}_2 T = A_{zx20}T
\end{cases}
\quad , \text{ (A17a)}
$$

for anisotropic case

$$
\begin{cases}
\varepsilon_{x20} = (\bar{a}_2^2 C_{11} + \bar{b}_2^2 C_{12} + \bar{c}_2^2 C_{13} + \bar{a}_2\bar{b}_2 C_{14} + \bar{b}_2\bar{c}_2 C_{15} + \bar{a}_2\bar{c}_2 C_{16})T = A_{x20}T \\
\varepsilon_{y20} = (\bar{a}_2^2 C_{21} + \bar{b}_2^2 C_{22} + \bar{c}_2^2 C_{23} + \bar{a}_2\bar{b}_2 C_{24} + \bar{b}_2\bar{c}_2 C_{25} + \bar{a}_2\bar{c}_2 C_{26})T = A_{y20}T \\
\varepsilon_{z20} = (\bar{a}_2^2 C_{31} + \bar{b}_2^2 C_{32} + \bar{c}_2^2 C_{33} + \bar{a}_2\bar{b}_2 C_{34} + \bar{b}_2\bar{c}_2 C_{35} + \bar{a}_2\bar{c}_2 C_{36})T = A_{z20}T \\
\gamma_{xy20} = (\bar{a}_2^2 C_{41} + \bar{b}_2^2 C_{42} + \bar{c}_2^2 C_{43} + \bar{a}_2\bar{b}_2 C_{44} + \bar{b}_2\bar{c}_2 C_{45} + \bar{a}_2\bar{c}_2 C_{46})T = A_{xy20}T \\
\gamma_{yz20} = (\bar{a}_2^2 C_{51} + \bar{b}_2^2 C_{52} + \bar{c}_2^2 C_{53} + \bar{a}_2\bar{b}_2 C_{54} + \bar{b}_2\bar{c}_2 C_{55} + \bar{a}_2\bar{c}_2 C_{56})T = A_{yz20}T \\
\gamma_{zx20} = (\bar{a}_2^2 C_{61} + \bar{b}_2^2 C_{62} + \bar{c}_2^2 C_{63} + \bar{a}_2\bar{b}_2 C_{64} + \bar{b}_2\bar{c}_2 C_{65} + \bar{a}_2\bar{c}_2 C_{66})T = A_{zx20}T
\end{cases}
\quad \text{(A17b)}
$$

(9) The 21st set of solutions for global stresses and strains

Stresses:

$$
\sigma_{x21} = 2\bar{a}_1\bar{a}_2 T, \quad \sigma_{y21} = 2\bar{b}_1\bar{b}_2 T, \quad \sigma_{z21} = 2\bar{c}_1\bar{c}_2 T, \quad \tau_{xy21} = h_9 T, \quad \tau_{yz21} = h_7 T, \quad \tau_{zx21} = h_8 T ; \quad \text{(A18)}
$$

Strains:

for isotropic case

$$
\begin{cases}
\varepsilon_{x21} = \dfrac{2}{E}(\bar{a}_1\bar{a}_2 - \mu\bar{b}_1\bar{b}_2 - \mu\bar{c}_1\bar{c}_2)T = A_{x21}T, \quad & \varepsilon_{y21} = \dfrac{2}{E}(\bar{b}_1\bar{b}_2 - \mu\bar{a}_1\bar{a}_2 - \mu\bar{c}_1\bar{c}_2)T = A_{y21}T \\[2mm]
\varepsilon_{z21} = \dfrac{2}{E}(\bar{c}_1\bar{c}_2 - \mu\bar{a}_1\bar{a}_2 - \mu\bar{b}_1\bar{b}_2)T = A_{z21}T, \quad & \gamma_{xy21} = \dfrac{2(1+\mu)}{E}(\bar{a}_1\bar{b}_2 + \bar{a}_2\bar{b}_1)T = A_{xy21}T \\[2mm]
\gamma_{yz21} = \dfrac{2(1+\mu)}{E}(\bar{b}_1\bar{c}_2 + \bar{b}_2\bar{c}_1)T = A_{yz21}T, \quad & \gamma_{zx21} = \dfrac{2(1+\mu)}{E}(\bar{a}_1\bar{c}_2 + \bar{a}_2\bar{c}_1)T = A_{zx21}T
\end{cases}
\quad , \text{(A19a)}
$$

for anisotropic case

$$
\begin{cases}
\varepsilon_{x21} = (2\bar{a}_1\bar{a}_2 C_{11} + 2\bar{b}_1\bar{b}_2 C_{12} + 2\bar{c}_1\bar{c}_2 C_{13} + h_9 C_{14} + h_7 C_{15} + h_8 C_{16})T = A_{x21}T \\
\varepsilon_{y21} = (2\bar{a}_1\bar{a}_2 C_{21} + 2\bar{b}_1\bar{b}_2 C_{22} + 2\bar{c}_1\bar{c}_2 C_{23} + h_9 C_{24} + h_7 C_{25} + h_8 C_{26})T = A_{y21}T \\
\varepsilon_{z21} = (2\bar{a}_1\bar{a}_2 C_{31} + 2\bar{b}_1\bar{b}_2 C_{32} + 2\bar{c}_1\bar{c}_2 C_{33} + h_9 C_{34} + h_7 C_{35} + h_8 C_{36})T = A_{z21}T \\
\gamma_{xy21} = (2\bar{a}_1\bar{a}_2 C_{41} + 2\bar{b}_1\bar{b}_2 C_{42} + 2\bar{c}_1\bar{c}_2 C_{43} + h_9 C_{44} + h_7 C_{45} + h_8 C_{46})T = A_{xy21}T \\
\gamma_{yz21} = (2\bar{a}_1\bar{a}_2 C_{51} + 2\bar{b}_1\bar{b}_2 C_{52} + 2\bar{c}_1\bar{c}_2 C_{53} + h_9 C_{54} + h_7 C_{55} + h_8 C_{56})T = A_{yz21}T \\
\gamma_{zx21} = (2\bar{a}_1\bar{a}_2 C_{61} + 2\bar{b}_1\bar{b}_2 C_{62} + 2\bar{c}_1\bar{c}_2 C_{63} + h_9 C_{64} + h_7 C_{65} + h_8 C_{66})T = A_{zx21}T
\end{cases}
. \tag{A19b}
$$

2. Nine sets of analytical general solutions for quadratic displacements in terms of R, S and T

(1) The 13th~15th sets of solutions for displacements (i=13~15)

$$
\begin{aligned}
U_i = \frac{1}{2J_0}\{ & [\bar{a}_1 J_0 A_{xi} + (J_0 - \bar{a}_1 a_1)(\bar{a}_1 A_{xi} + \bar{b}_1 A_{xyi} + \bar{c}_1 A_{zxi}) - a_1(\bar{b}_1^2 A_{yi} + \bar{c}_1^2 A_{zi} + \bar{b}_1\bar{c}_1 A_{yzi})]R^2 - a_1(\bar{a}_2^2 A_{xi} \\
& + \bar{b}_2^2 A_{yi} + \bar{c}_2^2 A_{zi} + \bar{a}_2\bar{b}_2 A_{xyi} + \bar{b}_2\bar{c}_2 A_{yzi} + \bar{a}_2\bar{c}_2 A_{zxi})S^2 - a_1(\bar{a}_3^2 A_{xi} + \bar{b}_3^2 A_{yi} + \bar{c}_3^2 A_{zi} + \bar{a}_3\bar{b}_3 A_{xyi} + \bar{b}_3\bar{c}_3 A_{yzi} \\
& + \bar{a}_3\bar{c}_3 A_{zxi})T^2 + [J_0(2\bar{a}_2 A_{xi} + \bar{b}_2 A_{xyi} + \bar{c}_2 A_{zxi}) - 2a_1(\bar{a}_1\bar{a}_2 A_{xi} + \bar{b}_1\bar{b}_2 A_{yi} + \bar{c}_1\bar{c}_2 A_{zi}) - a_1(h_9 A_{xyi} + h_7 A_{yzi} \\
& + h_8 A_{zxi})]RS + [J_0(2\bar{a}_3 A_{xi} + \bar{b}_3 A_{xyi} + \bar{c}_3 A_{zxi}) - 2a_1(\bar{a}_1\bar{a}_3 A_{xi} + \bar{b}_1\bar{b}_3 A_{yi} + \bar{c}_1\bar{c}_3 A_{zi}) - a_1(h_6 A_{xyi} + h_4 A_{yzi} \\
& + h_5 A_{zxi})]RT - a_1(2\bar{a}_2\bar{a}_3 A_{xi} + 2\bar{b}_2\bar{b}_3 A_{yi} + 2\bar{c}_2\bar{c}_3 A_{zi} + h_3 A_{xyi} + h_1 A_{yzi} + h_2 A_{zxi})ST \}
\end{aligned}
$$

(A20a)

$$
\begin{aligned}
V_i = \frac{1}{2J_0}\{ & [\bar{b}_1 J_0 A_{yi} + (J_0 - \bar{b}_1 b_1)(\bar{a}_1 A_{xyi} + \bar{b}_1 A_{yi} + \bar{c}_1 A_{yzi}) - b_1(\bar{a}_1^2 A_{xi} + \bar{c}_1^2 A_{zi} + \bar{a}_1\bar{c}_1 A_{zxi})]R^2 - b_1(\bar{a}_2^2 A_{xi} \\
& + \bar{b}_2^2 A_{yi} + \bar{c}_2^2 A_{zi} + \bar{a}_2\bar{b}_2 A_{xyi} + \bar{b}_2\bar{c}_2 A_{yzi} + \bar{a}_2\bar{c}_2 A_{zxi})S^2 - b_1(\bar{a}_3^2 A_{xi} + \bar{b}_3^2 A_{yi} + \bar{c}_3^2 A_{zi} + \bar{a}_3\bar{b}_3 A_{xyi} + \bar{b}_3\bar{c}_3 A_{yzi} \\
& + \bar{a}_3\bar{c}_3 A_{zxi})T^2 + [J_0(\bar{a}_2 A_{xyi} + 2\bar{b}_2 A_{yi} + \bar{c}_2 A_{yzi}) - 2b_1(\bar{a}_1\bar{a}_2 A_{xi} + \bar{b}_1\bar{b}_2 A_{yi} + \bar{c}_1\bar{c}_2 A_{zi}) - b_1(h_9 A_{xyi} + h_7 A_{yzi} \\
& + h_8 A_{zxi})]RS + [J_0(\bar{a}_3 A_{xyi} + 2\bar{b}_3 A_{yi} + \bar{c}_3 A_{yzi}) - 2b_1(\bar{a}_1\bar{a}_3 A_{xi} + \bar{b}_1\bar{b}_3 A_{yi} + \bar{c}_1\bar{c}_3 A_{zi}) - b_1(h_6 A_{xyi} + h_4 A_{yzi} \\
& + h_5 A_{zxi})]RT - b_1(2\bar{a}_2\bar{a}_3 A_{xi} + 2\bar{b}_2\bar{b}_3 A_{yi} + 2\bar{c}_2\bar{c}_3 A_{zi} + h_3 A_{xyi} + h_1 A_{yzi} + h_2 A_{zxi})ST \}
\end{aligned}
$$

(A20b)

$$
\begin{aligned}
W_i = \frac{1}{2J_0}\{ & [\bar{c}_1 J_0 A_{zi} + (J_0 - \bar{c}_1 c_1)(\bar{a}_1 A_{zxi} + \bar{b}_1 A_{yzi} + \bar{c}_1 A_{zi}) - \bar{c}_1(\bar{a}_1^2 A_{xi} + \bar{b}_1^2 A_{yi} + \bar{a}_1\bar{b}_1 A_{xyi})]R^2 - c_1(\bar{a}_2^2 A_{xi} \\
& + \bar{b}_2^2 A_{yi} + \bar{c}_2^2 A_{zi} + \bar{a}_2\bar{b}_2 A_{xyi} + \bar{b}_2\bar{c}_2 A_{yzi} + \bar{a}_2\bar{c}_2 A_{zxi})S^2 - c_1(\bar{a}_3^2 A_{xi} + \bar{b}_3^2 A_{yi} + \bar{c}_3^2 A_{zi} + \bar{a}_3\bar{b}_3 A_{xyi} + \bar{b}_3\bar{c}_3 A_{yzi} \\
& + \bar{a}_3\bar{c}_3 A_{zxi})T^2 + [J_0(\bar{a}_2 A_{zxi} + \bar{b}_2 A_{yzi} + 2\bar{c}_2 A_{zi}) - 2c_1(\bar{a}_1\bar{a}_2 A_{xi} + \bar{b}_1\bar{b}_2 A_{yi} + \bar{c}_1\bar{c}_2 A_{zi}) - c_1(h_9 A_{xyi} + h_7 A_{yzi} \\
& + h_8 A_{zxi})]RS + [J_0(\bar{a}_3 A_{zxi} + \bar{b}_3 A_{yzi} + 2\bar{c}_3 A_{zi}) - 2c_1(\bar{a}_1\bar{a}_3 A_{xi} + \bar{b}_1\bar{b}_3 A_{yi} + \bar{c}_1\bar{c}_3 A_{zi}) - c_1(h_6 A_{xyi} + h_4 A_{yzi} \\
& + h_5 A_{zxi})]RT - c_1(2\bar{a}_2\bar{a}_3 A_{xi} + 2\bar{b}_2\bar{b}_3 A_{yi} + 2\bar{c}_2\bar{c}_3 A_{zi} + h_3 A_{xyi} + h_1 A_{yzi} + h_2 A_{zxi})ST \}
\end{aligned}
$$

(A20c)

(2) The 16th~18th sets of solutions for displacements (i=16~18)

$$U_i = \frac{1}{2J_0}\{-a_2(\bar{a}_1^2 A_{xi} + \bar{b}_1^2 A_{yi} + \bar{c}_1^2 A_{zi} + \bar{a}_1\bar{b}_1 A_{xyi} + \bar{b}_1\bar{c}_1 A_{yzi} + \bar{a}_1\bar{c}_1 A_{zxi})R^2 + [\bar{a}_2 J_0 A_{xi} + (J_0 - \bar{a}_2 a_2)(\bar{a}_2 A_{xi}$$
$$+ \bar{b}_2 A_{xyi} + \bar{c}_2 A_{zxi}) - a_2(\bar{b}_2^2 A_{yi} + \bar{c}_2^2 A_{zi} + \bar{b}_2\bar{c}_2 A_{yzi})]S^2 - a_2(\bar{a}_3^2 A_{xi} + \bar{b}_3^2 A_{yi} + \bar{c}_3^2 A_{zi} + \bar{a}_3\bar{b}_3 A_{xyi} + \bar{b}_3\bar{c}_3 A_{yzi}$$
$$+ \bar{a}_3\bar{c}_3 A_{zxi})T^2 + [J_0(2\bar{a}_1 A_{xi} + \bar{b}_1 A_{xyi} + \bar{c}_1 A_{zxi}) - 2a_2(\bar{a}_1\bar{a}_2 A_{xi} + \bar{b}_1\bar{b}_2 A_{yi} + \bar{c}_1\bar{c}_2 A_{zi}) - a_2(h_9 A_{xyi} + h_7 A_{yzi}$$
$$+ h_8 A_{zxi})]RS - a_2(2\bar{a}_1\bar{a}_3 A_{xi} + 2\bar{b}_1\bar{b}_3 A_{yi} + 2\bar{c}_1\bar{c}_3 A_{zi} + h_6 A_{xyi} + h_4 A_{yzi} + h_5 A_{zxi})RT + [J_0(2\bar{a}_3 A_{xi} + \bar{b}_3 A_{xyi}$$
$$+ \bar{c}_3 A_{zxi}) - 2a_2(\bar{a}_2\bar{a}_3 A_{xi} + \bar{b}_2\bar{b}_3 A_{yi} + \bar{c}_2\bar{c}_3 A_{zi}) - a_2(h_3 A_{xyi} + h_1 A_{yzi} + h_2 A_{zxi})]ST\}$$

(A21a)

$$V_i = \frac{1}{2J_0}\{-b_2(\bar{a}_1^2 A_{xi} + \bar{b}_1^2 A_{yi} + \bar{c}_1^2 A_{zi} + \bar{a}_1\bar{b}_1 A_{xyi} + \bar{b}_1\bar{c}_1 A_{yzi} + \bar{a}_1\bar{c}_1 A_{zxi})R^2 + [\bar{b}_2 J_0 A_{yi} + (J_0 - \bar{b}_2 b_2)(\bar{a}_2 A_{xyi}$$
$$+ \bar{b}_2 A_{yi} + \bar{c}_2 A_{yzi}) - b_2(\bar{a}_2^2 A_{xi} + \bar{c}_2^2 A_{zi} + \bar{a}_2\bar{c}_2 A_{zxi})]S^2 - b_2(\bar{a}_3^2 A_{xi} + \bar{b}_3^2 A_{yi} + \bar{c}_3^2 A_{zi} + \bar{a}_3\bar{b}_3 A_{xyi} + \bar{b}_3\bar{c}_3 A_{yzi}$$
$$+ \bar{a}_3\bar{c}_3 A_{zxi})T^2 + [J_0(\bar{a}_1 A_{xyi} + 2\bar{b}_1 A_{yi} + \bar{c}_1 A_{yzi}) - 2b_2(\bar{a}_1\bar{a}_2 A_{xi} + \bar{b}_1\bar{b}_2 A_{yi} + \bar{c}_1\bar{c}_2 A_{zi}) - b_2(h_9 A_{xyi} + h_7 A_{yzi}$$
$$+ h_8 A_{zxi})]RS - b_2(2\bar{a}_1\bar{a}_3 A_{xi} + 2\bar{b}_1\bar{b}_3 A_{yi} + 2\bar{c}_1\bar{c}_3 A_{zi} + h_6 A_{xyi} + h_4 A_{yzi} + h_5 A_{zxi})RT + [J_0(\bar{a}_3 A_{xyi} + 2\bar{b}_3 A_{yi}$$
$$+ \bar{c}_3 A_{yzi}) - 2b_2(\bar{a}_2\bar{a}_3 A_{xi} + \bar{b}_2\bar{b}_3 A_{yi} + \bar{c}_2\bar{c}_3 A_{zi}) - b_2(h_3 A_{xyi} + h_1 A_{yzi} + h_2 A_{zxi})]ST\}$$

(A21b)

$$W_i = \frac{1}{2J_0}\{-c_2(\bar{a}_1^2 A_{xi} + \bar{b}_1^2 A_{yi} + \bar{c}_1^2 A_{zi} + \bar{a}_1\bar{b}_1 A_{xyi} + \bar{b}_1\bar{c}_1 A_{yzi} + \bar{a}_1\bar{c}_1 A_{zxi})R^2 + [\bar{c}_2 J_0 A_{zi} + (J_0 - \bar{c}_2 c_2)(\bar{a}_2 A_{zxi}$$
$$+ \bar{b}_2 A_{yzi} + \bar{c}_2 A_{zi}) - c_2(\bar{a}_2^2 A_{xi} + \bar{b}_2^2 A_{yi} + \bar{a}_2\bar{b}_2 A_{xyi})]S^2 - c_2(\bar{a}_3^2 A_{xi} + \bar{b}_3^2 A_{yi} + \bar{c}_3^2 A_{zi} + \bar{a}_3\bar{b}_3 A_{xyi} + \bar{b}_3\bar{c}_3 A_{yzi}$$
$$+ \bar{a}_3\bar{c}_3 A_{zxi})T^2 + [J_0(\bar{a}_1 A_{zxi} + \bar{b}_1 A_{yzi} + 2\bar{c}_1 A_{zi}) - 2c_2(\bar{a}_1\bar{a}_2 A_{xi} + \bar{b}_1\bar{b}_2 A_{yi} + \bar{c}_1\bar{c}_2 A_{zi}) - c_2(h_9 A_{xyi} + h_7 A_{yzi}$$
$$+ h_8 A_{zxi})]RS - c_2(2\bar{a}_1\bar{a}_3 A_{xi} + 2\bar{b}_1\bar{b}_3 A_{yi} + 2\bar{c}_1\bar{c}_3 A_{zi} + h_6 A_{xyi} + h_4 A_{yzi} + h_5 A_{zxi})RT + [J_0(\bar{a}_3 A_{zxi} + \bar{b}_3 A_{yzi}$$
$$+ 2\bar{c}_3 A_{zi}) - 2c_2(\bar{a}_2\bar{a}_3 A_{xi} + \bar{b}_2\bar{b}_3 A_{yi} + \bar{c}_2\bar{c}_3 A_{zi}) - c_2(h_3 A_{xyi} + h_1 A_{yzi} + h_2 A_{zxi})]ST\}$$

(A21c)

(3) The 19th~21st sets of solutions for displacements (i=19~21)

$$U_i = \frac{1}{2J_0}\{-a_3(\bar{a}_1^2 A_{xi} + \bar{b}_1^2 A_{yi} + \bar{c}_1^2 A_{zi} + \bar{a}_1\bar{b}_1 A_{xyi} + \bar{b}_1\bar{c}_1 A_{yzi} + \bar{a}_1\bar{c}_1 A_{zxi})R^2 - a_3(\bar{a}_2^2 A_{xi} + \bar{b}_2^2 A_{yi} + \bar{c}_2^2 A_{zi}$$
$$+ \bar{a}_2\bar{b}_2 A_{xyi} + \bar{b}_2\bar{c}_2 A_{yzi} + \bar{a}_2\bar{c}_2 A_{zxi})S^2 + [\bar{a}_3 J_0 A_{xi} + (J_0 - \bar{a}_3 a_3)(\bar{a}_3 A_{xi} + \bar{b}_3 A_{xyi} + \bar{c}_3 A_{zxi}) - a_3(\bar{b}_3^2 A_{yi}$$
$$+ \bar{c}_3^2 A_{zi} + \bar{b}_3\bar{c}_3 A_{yzi})]T^2 - a_3(2\bar{a}_1\bar{a}_2 A_{xi} + 2\bar{b}_1\bar{b}_2 A_{yi} + 2\bar{c}_1\bar{c}_2 A_{zi} + h_9 A_{xyi} + h_7 A_{yzi} + h_8 A_{zxi})RS$$
$$+ [J_0(2\bar{a}_1 A_{xi} + \bar{b}_1 A_{xyi} + \bar{c}_1 A_{zxi}) - 2a_3(\bar{a}_1\bar{a}_3 A_{xi} + \bar{b}_1\bar{b}_3 A_{yi} + \bar{c}_1\bar{c}_3 A_{zi}) - a_3(h_6 A_{xyi} + h_4 A_{yzi} + h_5 A_{zxi})]RT$$
$$+ [J_0(2\bar{a}_2 A_{xi} + \bar{b}_2 A_{xyi} + \bar{c}_2 A_{zxi}) - 2a_3(\bar{a}_2\bar{a}_3 A_{xi} + \bar{b}_2\bar{b}_3 A_{yi} + \bar{c}_2\bar{c}_3 A_{zi}) - a_3(h_3 A_{xyi} + h_1 A_{yzi} + h_2 A_{zxi})]ST\}$$

(A22a)

$$V_i = \frac{1}{2J_0}\{-b_3(\bar{a}_1^2 A_{xi} + \bar{b}_1^2 A_{yi} + \bar{c}_1^2 A_{zi} + \bar{a}_1\bar{b}_1 A_{xyi} + \bar{b}_1\bar{c}_1 A_{yzi} + \bar{a}_1\bar{c}_1 A_{zxi})R^2 - b_3(\bar{a}_2^2 A_{xi} + \bar{b}_2^2 A_{yi} + \bar{c}_2^2 A_{zi}$$
$$+ \bar{a}_2\bar{b}_2 A_{xyi} + \bar{b}_2\bar{c}_2 A_{yzi} + \bar{a}_2\bar{c}_2 A_{zxi})S^2 + [\bar{b}_3 J_0 A_{yi} + (J_0 - \bar{b}_3 b_3)(\bar{a}_3 A_{xyi} + \bar{b}_3 A_{yi} + \bar{c}_3 A_{yzi}) - b_3(\bar{a}_3^2 A_{xi}$$
$$+ \bar{c}_3^2 A_{zi} + \bar{a}_3\bar{c}_3 A_{zxi})]T^2 - b_3(2\bar{a}_1\bar{a}_2 A_{xi} + 2\bar{b}_1\bar{b}_2 A_{yi} + 2\bar{c}_1\bar{c}_2 A_{zi} + h_9 A_{xyi} + h_7 A_{yzi} + h_8 A_{zxi})RS$$
$$+ [J_0(\bar{a}_1 A_{xyi} + 2\bar{b}_1 A_{yi} + \bar{c}_1 A_{yzi}) - 2b_3(\bar{a}_1\bar{a}_3 A_{xi} + \bar{b}_1\bar{b}_3 A_{yi} + \bar{c}_1\bar{c}_3 A_{zi}) - b_3(h_6 A_{xyi} + h_4 A_{yzi} + h_5 A_{zxi})]RT$$
$$+ [J_0(\bar{a}_2 A_{xyi} + 2\bar{b}_2 A_{yi} + \bar{c}_2 A_{yzi}) - 2b_3(\bar{a}_2\bar{a}_3 A_{xi} + \bar{b}_2\bar{b}_3 A_{yi} + \bar{c}_2\bar{c}_3 A_{zi}) - b_3(h_3 A_{xyi} + h_1 A_{yzi} + h_2 A_{zxi})]ST\},$$

(A22b)

$$W_i = \frac{1}{2J_0}\{-c_3(\bar{a}_1^2 A_{xi} + \bar{b}_1^2 A_{yi} + \bar{c}_1^2 A_{zi} + \bar{a}_1\bar{b}_1 A_{xyi} + \bar{b}_1\bar{c}_1 A_{yzi} + \bar{a}_1\bar{c}_1 A_{zxi})R^2 - c_3(\bar{a}_2^2 A_{xi} + \bar{b}_2^2 A_{yi} + \bar{c}_2^2 A_{zi}$$
$$+ \bar{a}_2\bar{b}_2 A_{xyi} + \bar{b}_2\bar{c}_2 A_{yzi} + \bar{a}_2\bar{c}_2 A_{zxi})S^2 + [\bar{c}_3 J_0 A_{zi} + (J_0 - \bar{c}_3 c_3)(\bar{a}_3 A_{zxi} + \bar{b}_3 A_{yzi} + \bar{c}_3 A_{zi}) - c_3(\bar{a}_3^2 A_{xi}$$
$$+ \bar{b}_3^2 A_{yi} + \bar{a}_3\bar{b}_3 A_{xyi})]T^2 - c_3(2\bar{a}_1\bar{a}_2 A_{xi} + 2\bar{b}_1\bar{b}_2 A_{yi} + 2\bar{c}_1\bar{c}_2 A_{zi} + h_9 A_{xyi} + h_7 A_{yzi} + h_8 A_{zxi})RS$$
$$+ [J_0(\bar{a}_1 A_{zxi} + \bar{b}_1 A_{yzi} + 2\bar{c}_1 A_{zi}) - 2c_3(\bar{a}_1\bar{a}_3 A_{xi} + \bar{b}_1\bar{b}_3 A_{yi} + \bar{c}_1\bar{c}_3 A_{zi}) - c_3(h_6 A_{xyi} + h_4 A_{yzi} + h_5 A_{zxi})]RT$$
$$+ [J_0(\bar{a}_2 A_{zxi} + \bar{b}_2 A_{yzi} + 2\bar{c}_2 A_{zi}) - 2c_3(\bar{a}_2\bar{a}_3 A_{xi} + \bar{b}_2\bar{b}_3 A_{yi} + \bar{c}_2\bar{c}_3 A_{zi}) - c_3(h_3 A_{xyi} + h_1 A_{yzi} + h_2 A_{zxi})]ST\}.$$

(A22c)

ACKNOWLEDGEMENTS

REFERENCES

1. *Abaqus 6.10 HTML Documentation*. Dassault Systèmes Simulia Corp. : Providence, RI, USA, 2010.
2. Wilson EL, Taylor RL, Doherty WP, Ghaboussi J. Incompatible displacement models. *Numerical and Computer Methods in Structural Mechanics*, Fenven ST et al. (Eds). Academic Press: New York, 1973; 43–57.
3. Taylor RL, Beresford PJ, Wilson EL. A non-conforming element for stress analysis. *International Journal for Numerical Methods in Engineering* 1976; **10**(6):1211–1219.
4. Simo JC, Hughes TJR. On the variational foundations of assumed strain methods. *Journal of Applied Mechanics*

1986; **53**(1):51–54.

5. Simo JC, Rifai MS. A class of mixed assumed strain methods and the method of incompatible modes. *International Journal for Numerical Methods in Engineering* 1990; **29**(8):1595–1638.

6. MacNeal RH. A theorem regarding the locking of tapered four-noded membrane elements. *International Journal for Numerical Methods in Engineering* 1987; **24**(9): 1793–1799.

7. MacNeal RH. On the limits of element perfectability. *International Journal for Numerical Methods in Engineering* 1992; **35**(8): 1589–1601.

8. Kavanagh KT, Key SW. A note on selective and reduced integration techniques in finite element method. *International Journal for Numerical Methods in Engineering* 1972; **4**:148–150.

9. Malkus DS, Hughes TJR. Mixed finite element methods−reduced and selective integration techniques: a unification of concepts. *Computer Methods in Applied Mechanics and Engineering* 1978; **15**(1):63–81.

10. Hughes TJR. Generalization of selective integration procedures to anisotropic and nonlinear media. *International Journal for Numerical Methods in Engineering* 1980; **15**(9):1413–1418.

11. Kosloff D, Frazier GA. Treatment of hourglass patterns in low order finite element codes. *International Journal for Numerical and Analytical Methods in Geomechanics* 1978; **2**(1):57–72.

12. Flanagan DP, Belytschko T. A uniform strain hexahedron and quadrilateral with orthogonal hourglass control. *International Journal for Numerical Methods in Engineering* 1981; **17**(5):679–706.

13. Belytschko T, Ong JSJ, Liu WK, Kennedy JM. Hourglass control in linear and nonlinear problems. *Computer Methods in Applied Mechanics and Engineering* 1984; **43**(3):251–276.

14. Koh BC, Kikuchi N. New improved hourglass control for bilinear and trilinear elements in anisotropic linear elasticity. *Computer Methods in Applied Mechanics and Engineering* 1987; **65**(1):1–46.

15. Belytschko T, Bindeman LP. Assumed strain stabilization of the eight node hexahedral element. *Computer Methods in Applied Mechanics and Engineering* 1993; **105**(2):225–260.

16. Fredriksson M, Ottosen NS. Accurate eight-node hexahedral element. *International Journal for Numerical Methods in Engineering* 2007; **72**(6):631–657.

17. Cheung YK, Chen WJ. Isoparametric hybrid hexahedral elements for three dimensional stress analysis. *International Journal for Numerical Methods in Engineering* 1988; **26**(3):677–693.

18. Cao YP, Hu N, Lu J, Fukunaga H, Yao ZH. A 3D brick element based on Hu−Washizu variational principle for mesh distortion. *International Journal for Numerical Methods in Engineering* 2002; **53**(11):2529–2548.

19. Bassayya K, Bhattacharya K, Shrinivasa U. Eight-node brick, PN340, represents constant stress fields exactly. *Computers & Structures* 2000; **74**(4):441–460.

20. Ooi ET, Rajendran S, Yeo JH, Zhang BR. A mesh distortion tolerant 8-node solid element based on the partition of unity method with inter-element compatibility and completeness properties. *Finite Elements in Analysis and Design* 2007; **43**(10):771–781.

21. Lee NS, Bathe KJ. Effects of element distortions on the performance of isoparametric elements. *International Journal for Numerical Methods in Engineering* 1993; **36**(20):3553–3576.

22. Long YQ, Cen S, Long ZF. *Advanced Finite Element Method in Structural Engineering*. Springer-Verlag GmbH: Berlin, Heidelberg; Tsinghua University Press: Beijing, 2009.

23. Long YQ, Li JX, Long ZF, Cen S. Area co-ordinates used in quadrilateral elements. *Communications in Numerical Methods in Engineering* 1999; **15**(8):533–545.

24. Long ZF, Li JX, Cen S, Long YQ. Some basic formulae for area co-ordinates used in quadrilateral elements. *Communications in Numerical Methods in Engineering* 1999; **15**(12):841–852.

25. Chen XM, Cen S, Fu XR, Long YQ. A new quadrilateral area coordinate method (QACM-II) for developing quadrilateral finite element models. *International Journal for Numerical Methods in Engineering* 2008; **73**(13): 1911–1941.

26. Long ZF, Cen S, Wang L, Fu XR, Long YQ. The third form of the quadrilateral area coordinate method (QACM-III): theory, application, and scheme of composite coordinate interpolation. *Finite Elements in Analysis and Design* 2010; **46**(10):805–818.

27. Li HG, Cen S, Cen ZZ. Hexahedral volume coordinate method (HVCM) and improvements on 3D Wilson hexahedral element. *Computer Methods in Applied Mechanics and Engineering* 2008; **197**(51-52):4531–4548.

28. Chen XM, Cen S, Long YQ, Yao ZH. Membrane elements insensitive to distortion using the quadrilateral area coordinate method. *Computers & Structures* 2004; **82**(1):35–54.

29. Cen S, Chen XM, Fu XR. Quadrilateral membrane element family formulated by the quadrilateral area coordinate method. *Computer Methods in Applied Mechanics and Engineering* 2007; **196**(41-44):4337–4353.

30. Cen S, Du Y, Chen XM, Fu XR. The analytical element stiffness matrix of a recent 4-node membrane element formulated by the quadrilateral area coordinate method. *Communications in Numerical Methods in Engineering* 2007; **23**(12):1095–1110.

31. Du Y, Cen S. Geometrically nonlinear analysis with a 4-node membrane element formulated by the quadrilateral area coordinate method. *Finite Elements in Analysis and Design* 2008; **44**(8):427–438.

32. Cen S, Chen XM, Li CF, Fu XR. Quadrilateral membrane elements with analytical element stiffness matrices formulated by the new quadrilateral area coordinate method (QACM-II). *International Journal for Numerical Methods in Engineering* 2009; **77**(8):1172–1200.

33. Li G. A four-node plane parametric element based on quadrilateral area coordinate and its application to coupled solid-deformation/fluid-flow simulation for porous geomaterials. *International Journal for Numerical and Analytical Methods in Geomechanics* 2015; **39**(3): 251– 276.

34. Flajs R, Cen S, Saje M. On convergence of nonconforming convex quadrilateral finite elements AGQ6. *Computer Methods in Applied Mechanics and Engineering* 2010; **199**(25-28):1816–1827.

35. Prathap G, Senthilkumar V. Making sense of the quadrilateral area coordinate membrane elements. *Computer Methods in Applied Mechanics and Engineering* 2008; **197**(49-50): 4379–4382.

36. Chen XM, Cen S, Li YG, Sun JY. Several treatments on non-conforming element failed in the strict patch test. *Mathematical Problems in Engineering* 2013; 901495.

37. Rajendran S, Liew KM. A novel unsymmetric 8-node plane element immune to mesh distortion under a quadratic displacement field. *International Journal for Numerical Methods in Engineering* 2003; **58**(11):1713–1748.

38. Ooi ET, Rajendran S, Yeo JH. A 20-node hexahedral element with enhanced distortion tolerance. *International Journal for Numerical Methods in Engineering* 2004; **60**(15):2501–2530.

39. Liew KM, Rajendran S, Wang J. A quadratic plane triangular element immune to quadratic mesh distortions under quadratic displacement fields. *Computer Methods in Applied Mechanics and Engineering* 2006; **195**(9-12): 1207–1223.

40. Ooi ET. Rajendran S, Yeo JH. Extension of unsymmetric finite elements US-QUAD8 and US-HEXA20 for geometric nonlinear analyses. *Engineering Computations* 2007; **24**(4):407–431.

41. Rajendran S. A technique to develop mesh-distortion immune finite elements. *Computer Methods in Applied Mechanics and Engineering* 2010; **199**(17-20):1044–1063.

42. Rajendran S, Ooi ET, Yeo JH. Mesh-distortion immunity assessment of QUAD8 elements by strong-form patch tests. *Communications in Numerical Methods in Engineering* 2007; **23** (2):157–168.

43. Ooi ET, Rajendran S, Yeo JH. Remedies to rotational frame dependence and interpolation failure of US-QUAD8 element. *Communications in Numerical Methods in Engineering* 2008; **24**(11):1203–1217.

44. Cen S, Zhou GH, Fu XR. A shape-free 8-node plane element unsymmetric analytical trial function method. *International Journal for Numerical Methods in Engineering* 2012; **91**(2):158–185.

45. Cen S, Zhou PL, Li CF, Wu CJ. An unsymmetric 4-node, 8-DOF plane membrane element perfectly breaking through MacNeal's theorem. *International Journal for Numerical Methods in Engineering* 2015; **103**(7):469–500.

46. Xie Q, Sze KY, Zhou YX. Modified and trefftz unsymmetric finite element models. *International Journal of Mechanics and Materials in Design* 2016; **12**(1):53–70.

47. Yuan KY, Huang YS, Pian THH. New strategy for assumed stresses for 4-node hybrid stress membrane element. *International Journal for Numerical Methods in Engineering* 1993; **36**(10):1747–1763.

48. Yuan KY, Huang YS, Yang HT, Pian THH. The inverse mapping and distortion measures for 8-node hexahedral isoparametric elements. *Computational Mechanics* 1994; **14**(2): 189–199.

49. Qin QH. Trefftz finite element method and its applications. *Applied Mechanics Reviews* 2005; **58**(5):316–337.

50. Cen S, Fu XR, Zhou MJ. 8- and 12-node plane hybrid stress-function elements immune to severely distorted mesh containing elements with concave shapes. *Computer Methods in Applied Mechanics and Engineering* 2011; **200**(29-32):2321–2336.

51. Cen S, Fu XR, Zhou GH, Zhou MJ, Li CF. Shape-free finite element method: The plane hybrid stress-function (HS-F) element method for anisotropic materials. *SCIENCE CHINA Physics, Mechanics & Astronomy* 2011; **54**(4): 653–665.

52. Cen S, Zhou MJ, Fu XR. A 4-node hybrid stress-function (HS-F) plane element with drilling degrees of freedom less sensitive to severe mesh distortions. *Computers & Structures* 2011; **89**(5-6):517–528.

53. Cen S, Zhou MJ, Shang Y. Shape-free finite element method: another way between mesh and mesh-free methods. *Mathematical Problems in Engineering* 2013; **2013**:491626.

54. Zhou MJ, Cen S, Bao Y, Li CF. A quasi-static crack propagation simulation based on shape-free hybrid stress-function finite elements with simple remeshing. *Computer Methods in Applied Mechanics and Engineering* 2014; **275**:159–188.

55. Zhou PL, Cen S. A novel shape-free plane quadratic polygonal hybrid stress-function element. *Mathematical Problems in Engineering* 2015; **2015**: 491325.

56. Cook RD, Malkus DS, Plesha ME. *Concepts and Applications of Finite Element Analysis* (3rd Edn). New York: John Wiley & Sons, Inc.; 1989.

57. MacNeal RH, Harder RL. A proposed standard set of problems to test finite element accuracy. *Finite Elements in Analysis and Design* 1985; **1**(1): 3–20.

58. *INTESIM 2014 Theory Manual*. Intesim Group: Venetia, PA, USA, 2014.

Table 1. The first 27 sets of analytical general solutions for stresses in terms of 3D oblique coordinate system

i	1	2	3	4	5	6	7	8	9	10	11	12
Corresponding displacements	Rigid body displacement modes			Linear displacement modes								
u_i	1	0	0	R	0	0	S	0	0	T	0	0
v_i	0	1	0	0	R	0	0	S	0	0	T	0
w_i	0	0	1	0	0	R	0	0	S	0	0	T
σ_{Ri}	0	0	0									
σ_{Si}	0	0	0									
σ_{Ti}	0	0	0				Constant Stress solutions					
τ_{RSi}	0	0	0									
τ_{STi}	0	0	0									
τ_{RTi}	0	0	0									

i	13	14	15	16	17	18	19	20	21	22	23	24	25	26	27
Corresponding displacements	Quadratic displacement modes														
σ_{Ri}	0	0	0	S	0	0	T	0	0	0	$-R$	0	0	0	$-R$
σ_{Si}	R	0	0	0	0	0	0	T	0	$-S$	0	0	$-S$	0	0
σ_{Ti}	0	R	0	0	S	0	0	0	0	0	0	$-T$	0	$-T$	0
τ_{RSi}	0	0	0	0	0	0	0	0	T	R	S	0	0	0	0
τ_{STi}	0	0	R	0	0	0	0	0	0	0	0	S	T	0	0
τ_{RTi}	0	0	0	0	0	S	0	0	0	0	0	0	0	R	T

Table 2. List of element models for comparison.

No.	Symbol	Explanation of elements	References
1	C3D8	8-node tri-linear hexahedral element with full integration in ABAQUS	[1]
2	C3D8R	8-node tri-linear hexahedral element with reduced integration and hourglass control in ABAQUS	[1]
3	C3D8I	8-node incompatible hexahedral element in ABAQUS	[1]
4	C3D8H	8-node hybrid hexahedral element in ABAQUS	[1]
5	Wilson_H8	8-node incompatible hexahedral element by Wilson's method	[2]
6	HEXA(8)	8-node hexahedral element by MacNeal et al.	[56]
7	ASQBI	8-node hexahedral element by Belytschko and Bindeman	[15]
8	NEWHEX	8-node brick element based on EAS method	[16]
9	HVCC8/ -ES/ EM	8-node incompatible hexahedral elements using hexahedral volume coordinate method and cannot strictly pass the constant strain patch test.	[27]
10	TH8	Unsymmetric 8-node hexahedral element with adjustable factor β (=0.01)	[46]

Table 3. The x coordinates of nodes 1, 2, 3 and 4 in Meshes (2) to (10) (Figure 4).

x-coordinates	Meshes								
	(2)	(3)	(4)	(5)	(6)	(7)	(8)	(9)	(10)
x_1	5	5	5	5	2	2	6	8	8
x_2	5	5	4	6	8	5	5	5	8
x_3	5	6	5	6	8	5	5	6	8
x_4	5	6	6	5	2	8	8	2	2

Table 4. The normalized deflections at point A for Cheung and Chen tests (Figure 4).

Model / Mesh	C3D8	C3D8R	C3D8I	Wilson_H8	HVCC8	TH8 β=0.01	TH8 β=0.0001	US-ATFH8
Load *M*: normalized deflections at point A, exact solution: 100								
(1)	0.0956	1.0000	1.0000	1.0000	1.0000	1.0000	1.0000	**1.0000**
(2)	0.3382	1.0000	1.0000	1.0000	1.0000	1.0000	1.0000	**1.0000**
(3)	0.2684	0.8756	0.8931	0.9397	1.0027	1.0000	1.0000	**1.0000**
(4)	0.2529	0.7652	0.7911	0.8962	1.0020	1.0000	1.0000	**1.0000**
(5)	0.2441	0.7738	0.7717	0.8836	1.0000	1.0000	1.0000	**1.0000**
(6)	0.0919	0.4516	0.4085	0.7875	1.0000	1.0000	1.0000	**1.0000**
(7)	0.1435	7.0712	0.2638	—	—	1.0000	1.0000	**1.0000**
(8)	0.1570	11.4629	0.5900	—	—	1.0000	1.0000	**1.0000**
(9)	0.1322	6.8514	0.1923	—	—	1.0000	1.0000	**1.0000**
(10)	0.0956	4.4017	0.2111	—	—	1.0000	1.0000	**1.0000**
(11)	0.8013	0.9956	0.9578	0.9826	1.0000	1.0000	1.0000	**1.0000**
(12)	0.6905	46.0988	0.7228	—	—	1.0000	1.0000	**1.0000**
Load *P*: normalized displacements at point A, exact solution: 102.6								
(1)	0.0942	0.7554	0.7554	0.7554	0.7554	0.7554	0.7554	**0.7554**
(2)	0.3329	0.9367	0.9353	0.9340	0.9340	0.9380	0.9381	**0.9340**
(3)	0.2648	0.8440	0.8445	0.8773	0.9254	0.9370	0.9358	**0.9262**
(4)	0.2692	0.7650	0.7696	0.8479	0.9295	0.9378	0.9367	**0.9270**
(5)	0.2485	0.7694	0.7658	0.8491	0.9383	0.9380	0.9381	**0.9343**
(6)	0.1330	0.5368	0.4800	0.8723	1.2292	1.0038	1.0039	**1.0135**
(7)	0.1829	22.2781	0.3260	—	—	0.8595	0.8586	**0.8615**
(8)	0.1787	23.9254	0.6263	—	—	0.9529	0.9491	**0.9929**
(9)	0.1713	21.3401	0.2803	—	—	0.8052	0.8002	**0.9026**
(10)	0.1275	18.0603	0.2549	—	—	0.7409	0.7368	**0.7062**
(11)	0.8690	0.9922	0.9536	0.9770	0.9999	0.9889	0.9889	**0.9875**
(12)	0.7733	49.7021	0.7717	—	—	0.9618	−2.6592	**0.9926**

Table 5. The results of stress at point B for Cheung and Chen tests (Figure 4).

Mesh / Model	C3D8	C3D8R	C3D8I	Wilson_H8	HVCC8	TH8 $\beta=0.01$	TH8 $\beta=0.0001$	**US-ATFH8**	Exact
Load M									
(1)	−131.1	2.51×10^{-12}	−3000	−3000	−3000	−3000	−3000	**−3000**	−3000
(2)	−463.8	9.99×10^{-13}	−3000	−3000	−3000	−3000	−3000	**−3000**	−3000
(3)	−377.7	-2.33×10^{-13}	−2632	−2775	−3007	−3000	−3000	**−3000**	−3000
(4)	−380.3	−24.16	−2249	−3161	−3003	−3000	−3000	**−3000**	−3000
(5)	−238.8	−18.30	−2404	−2251	−3000	−3000	−3000	**−3000**	−3000
(6)	−30.63	277.5	−1950	−241.3	−3000	−3000	−3000	**−3000**	−3000
(7)	−187.5	7.79×10^{-13}	−719.9	—	—	−3000	−3000	**−3000**	−3000
(8)	−270.8	−130.8	−1500	—	—	−3000	−3000	**−3000**	−3000
(9)	−154.6	40.72	−636.2	—	—	−3000	−3000	**−3000**	−3000
(10)	−82.50	204.1	−925.5	—	—	−3000	−3000	**−3000**	−3000
(11)	−1316	−321.9	−2999	−2340	−3000	−3000	−3000	**−3000**	−3000
(12)	−1266	−261.6	−2810	—	—	−3000	−3000	**−3000**	−3000
Load P									
(1)	−98.36	2.76×10^{-12}	−2250	−2250	−2250	−2250	−2250	**−2250**	−2250
(2)	−427.4	5.66×10^{-13}	−2841	−3375	−3375	−3375	−3375	**−3375**	−3375
(3)	−320.6	0.000	−2419	−3037.2	−3211.4	−3257.5	−3252.2	**−3229.6**	−3262.5
(4)	−360.9	−18.14	−2212	−3667	−3348	−3408.8	−3403.4	**−3373.5**	−3375
(5)	−219.6	−6.908	−2243	−2518	−3238	−3225	−3225	**−3226.6**	−3150
(6)	−57.09	208.1	−1823	−209.8	−3641	−3150	−3150	**−3198.9**	−2700
(7)	−332.1	755.3	−925.9	—	—	−2883.6	−2877.9	**−3038.6**	−3375
(8)	−229.5	−124.2	−1647	—	—	−3239.5	−3226.7	**−3369.9**	−3375
(9)	−292.2	22.04	−820.7	—	—	−2695.9	−2677.9	**−3083.2**	−3262.5
(10)	−109.1	197.0	−667.2	—	—	−2248.8	−2234.6	**−2170.9**	−2700
(11)	−1781	−371.0	−3947	−3234	−4179	−4125.4	−4125.4	**−4125.5**	−4050
(12)	−1746	−321.4	−3738	—	—	−4123.4	−4123.7	**−4125.3**	−4050

Table 6. The results of deflections at points a_1, a_2, a_3 and a_4 under load P (Figure 4).

Mesh	Node	TH8 β=0.01	TH8 β=0.0001	US-ATFH8
(7)	a_1	88.20	88.09	**88.39**
	a_2	88.18	88.09	**88.40**
	a_3	65.01	−2292.81	**88.87**
	a_4	112.29	2469.91	**88.97**
(8)	a_1	97.57	97.19	**100.44**
	a_2	97.77	97.38	**101.87**
	a_3	95.92	−11.72	**100.42**
	a_4	99.64	206.51	**102.01**
(9)	a_1	81.87	81.33	**91.71**
	a_2	82.62	82.10	**92.61**
	a_3	99.02	1694.96	**92.49**
	a_4	66.23	−1530.77	**92.59**
(10)	a_1	75.20	74.73	**69.19**
	a_2	76.01	75.60	**72.45**
	a_3	82.38	831.37	**69.54**
	a_4	69.15	−680.72	**72.38**
(12)	a_1	105.17	476.83	**102.35**
	a_2	98.68	−272.84	**101.84**
	a_3	102.04	102.14	**102.31**
	a_4	101.72	101.76	**101.77**

Reference solution: 102.6

Table 7. Results of the displacement at point A calculated for the rotational frame invariance test (Figure 5).

α_1	α_2	u_A	v_A	w_A	$\sqrt{u_A^2 + v_A^2 + w_A^2}$	Normalized
0°	0°	−0.235778E-01	−0.454176E-01	0.336472E-03	0.051174	0.96260
0°		−0.182779E-01	−0.454176E-01	−0.148978E-01	0.051174	0.96260
10°		−0.258869E-01	−0.415536E-01	−0.148978E-01	0.051174	0.96260
20°		−0.327094E-01	−0.364271E-01	−0.148978E-01	0.051174	0.96260
30°		−0.385379E-01	−0.301938E-01	−0.148978E-01	0.051174	0.96260
40°		−0.431956E-01	−0.230430E-01	−0.148978E-01	0.051174	0.96260
45°	40°	−0.450395E-01	−0.191906E-01	−0.148978E-01	0.051174	0.96260
50°		−0.465407E-01	−0.151921E-01	−0.148978E-01	0.051174	0.96260
60°		−0.484717E-01	−0.687962E-02	−0.148978E-01	0.051174	0.96260
70°		−0.489300E-01	0.164193E-02	−0.148978E-01	0.051174	0.96260
80°		−0.479015E-01	0.101136E-01	−0.148978E-01	0.051174	0.96260
90°		−0.454176E-01	0.182779E-01	−0.148978E-01	0.051174	0.96260
90°	90°	−0.454176E-01	0.336472E-03	−0.235778E-01	0.051174	0.96260
Overkill solution		—	—	—	0.053162	1.00000

Table 8. Results of Cook's skew beam problem (Figure 6).

Element	Mesh					
	2×2×1	2×2×2	4×4×4	8×8×4	8×8×8	16×16×16
Deflection at point C: v_C (reference solution: 23.86[a])						
C3D8	13.95	14.05	19.81	22.48	22.50	23.36
C3D8R	20.56	20.50	22.51	23.32	23.32	23.58
C3D8I	20.39	20.32	22.50	23.32	23.32	23.58
TH8 β=0.01	22.73	22.59	23.27	23.67	23.67	23.81
US-ATFH8	**22.67**	**22.56**	**23.27**	**23.67**	**23.67**	**23.81**
Maximum principle stress at point A: σ_{Amax} (reference solution: 0.2352[a])						
C3D8	0.1389	0.1423	0.1889	0.2164	0.2159	0.2267
C3D8R	0.1299	0.1300	0.1861	0.2138	0.2134	0.2248
C3D8I	0.1741	0.1746	0.2172	0.2320	0.2317	0.2340
TH8 β=0.01	0.1952	0.1949	0.2218	0.2326	0.2324	0.2345
US-ATFH8	**0.1973**	**0.1952**	**0.2214**	**0.2325**	**0.2322**	**0.2345**
Minimum principle stress at point B: σ_{Bmin} (reference solution: −0.2023[a])						
C3D8	−0.0970	−0.0974	−0.1337	−0.1747	−0.1727	−0.1912
C3D8R	−0.0664	−0.0664	−0.1282	−0.1666	−0.1663	−0.1848
C3D8I	−0.1689	−0.1664	−0.1804	−0.1976	−0.1963	−0.2013
TH8 β=0.01	−0.1548	−0.1534	−0.1869	−0.1979	−0.1977	−0.2013
US-ATFH8-A	**−0.1554**	**−0.1574**	**−0.1874**	**−0.1976**	**−0.1975**	**−0.2013**

[a] Results by traditional 20-node hexahedral isoparametric element using 46×46×46 mesh in Abaqus [1].

Table 9. Normalized deflections at point A for a thin curved beam subjected to an in-plane shear P_1 (Figure 7).

Number of elements	C3D8	C3D8R	C3D8I	ASQBI	NEWHEX	Wilson _H8	HVCC8	TH8 β=0.01	US-ATFH8
2	0.006	0.049	0.049	0.669	0.669	0.107	1.043	0.947	**0.909**
4	0.033	0.581	0.580	0.895	0.895	0.717	1.015	0.991	**0.974**
6	0.077	0.883	0.881	0.978	0.978	0.935	1.012	1.002	**0.992**
8	0.136	0.966	0.964	0.997	0.997	0.984	1.011	1.007	**0.999**
10	0.208	0.992	0.990	1.003	1.003	0.999	1.011	1.009	**1.003**
12	0.289	1.002	1.000	—	—	1.004	1.011	1.010	**1.005**
14	0.378	1.006	1.005	—	—	1.007	1.011	1.011	**1.007**
16	0.471	1.009	1.007	—	—	1.009	1.011	1.012	**1.008**
20	0.664	1.011	1.010	—	—	1.010	1.012	1.012	**1.009**
Analytical	1.000[a]								

[a] Standard solution: 0.08734.

Table 10. Normalized deflections at point A for a thin curved beam subjected to an out-of-plane shear P_2 (Figure 7).

Number of elements	C3D8	C3D8R	C3D8I	Wilson_H8	HVCC8	TH8 $\beta=0.01$	US-ATFH8
2	0.132	0.192	0.160	0.190	0.799	0.896	**0.968**
4	0.202	0.604	0.570	0.666	0.890	0.952	**0.934**
6	0.230	0.847	0.821	0.865	0.920	0.964	**0.945**
8	0.250	0.920	0.901	0.918	0.934	0.969	**0.952**
10	0.269	0.944	0.929	0.936	0.942	0.972	**0.956**
12	0.289	0.953	0.942	0.945	0.947	0.973	**0.960**
14	0.311	0.958	0.948	0.949	0.950	0.974	**0.962**
16	0.334	0.960	0.952	0.952	0.952	0.975	**0.964**
20	0.386	0.962	0.956	0.956	0.955	0.976	**0.966**
Analytical	1.000[a]						

[a] Standard solution: 0.5022.

Table 11. Normalized deflections at point A for a twisted beam subjected to an in-plane force (Figure 8).

Mesh	C3D8	C3D8I	TH8 β=0.01	US-ATFH8
4×2	0.0313	0.9750	1.0646	**1.0567**
8×2	0.1145	0.9911	1.0155	**1.0106**
8×4	0.1144	0.9977	1.0090	**1.0057**
16×2	0.3728	0.9967	1.0035	**1.0014**
16×4	0.3767	0.9992	1.0023	**1.0009**
16×8	0.3799	1.0000	1.0023	**1.0010**
(a)	0.0584	0.6137	1.0407	**1.0235**
(b)	0.0528	0.6238	1.0388	**1.0289**
(c)	0.0446	0.1024	1.1403	**1.0203**
(d)	0.0374	0.0842	1.3741	**0.7756**
Exact	1.0000[a]			

[a] The standard value is 0.005424.

Table 12. Normalized deflections at point A for a twisted beam subjected to an out-of-plane force (Figure 8).

Mesh	C3D8	C3D8I	TH8 $\beta=0.01$	US-ATFH8
4×2	0.0834	0.9246	1.0222	**1.0252**
8×2	0.2297	0.9780	1.0029	**1.0033**
8×4	0.2242	0.9820	0.9974	**0.9985**
16×2	0.4998	0.9926	0.9991	**0.9991**
16×4	0.4909	0.9942	0.9980	**0.9983**
16×8	0.4912	0.9947	0.9980	**0.9982**
(a)	0.1538	0.8886	0.9472	**0.9885**
(b)	0.1377	0.8925	0.9359	**0.9995**
(c)	0.1377	0.3056	1.0361	**1.0094**
(d)	0.1156	0.2679	1.1296	**1.0613**
Exact	1.0000[a]			

[a] The standard value is 0.001754.

Table 13. Normalized radial displacements at inner radius for a thick-walled cylinder (Figure 9).

Poisson's ratio	H8[a]	C3D8H	C3D8I	HEXA(8)	ASQBI	TH8 β=0.01	**US-ATFH8**
0.49	0.849	0.993	0.986	0.986	0.988	0.978	**0.978**
0.499	0.361	0.993	0.986	0.986	0.987	0.978	**0.978**
0.4999	0.053	0.993	0.986	0.986	0.987	0.978	**0.978**

[a] H8: The standard 8-node tri-linear isoparametric element
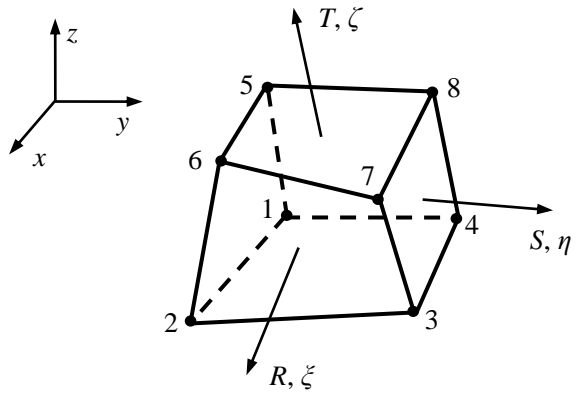
Figure 1. The definition of 3D oblique coordinate system.
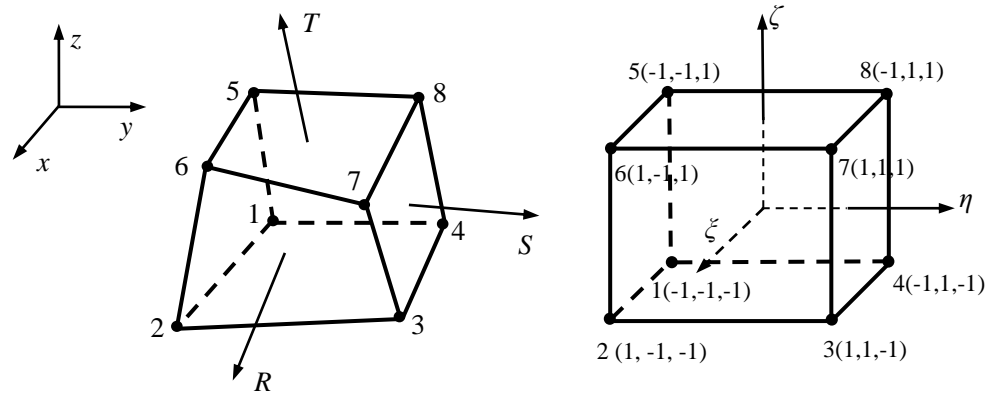
Figure 2. An 8-node hexahedral element.
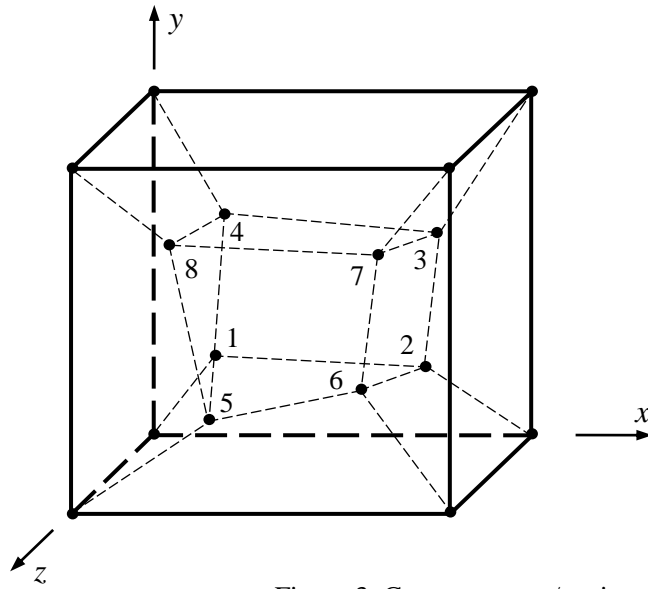
Node	Cartesian coordina	
	x	y
1	0.249	0.342
2	0.826	0.288
3	0.850	0.649
4	0.273	0.750
5	0.320	0.186
6	0.677	0.305
7	0.788	0.693
8	0.165	0.745

Figure 3. Constant stress/strain patch test.

Outer dimensions: unit cube; $E=1.0\times10^6$; $\mu=0.25$.
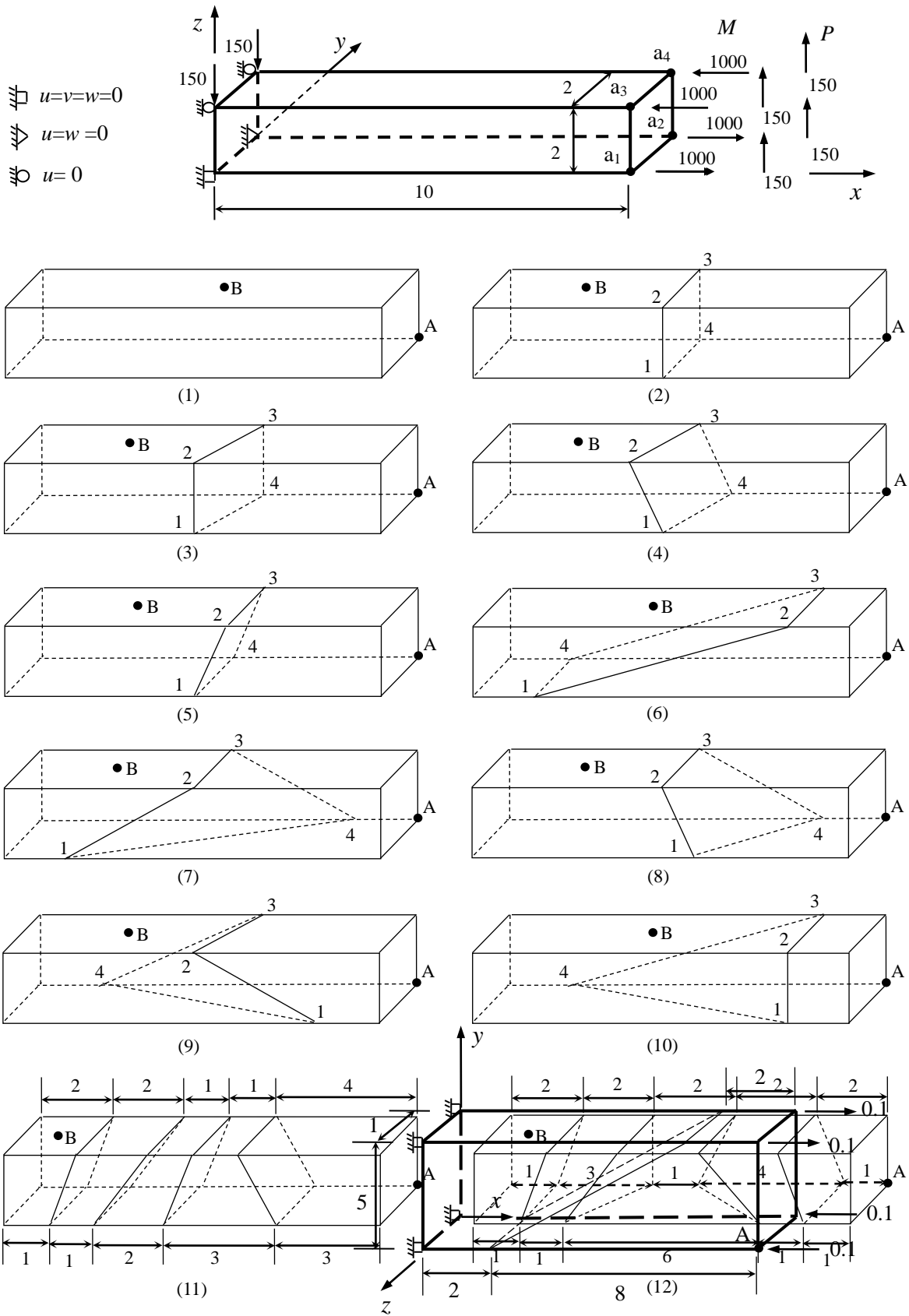
Figure 4. Cheung and Chen beam tests. $E=1500$; $\mu=0.25$

Figure 5. Rotation dependence test: cantilever beam problem and mesh. $E=100.0$; $\mu=0.3$.
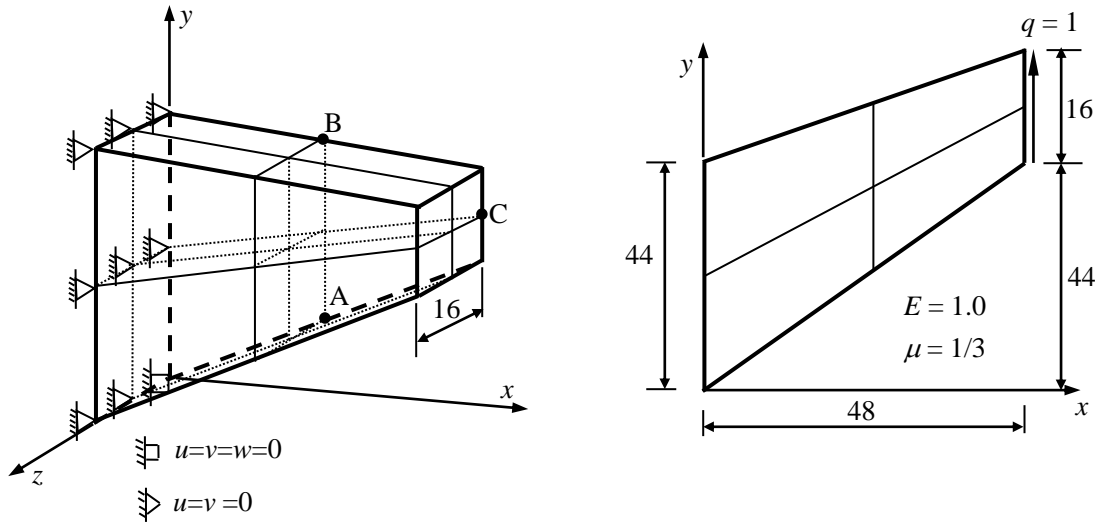
Figure 6. Cook's skew beam problem and a typical 2×2×2 mesh.
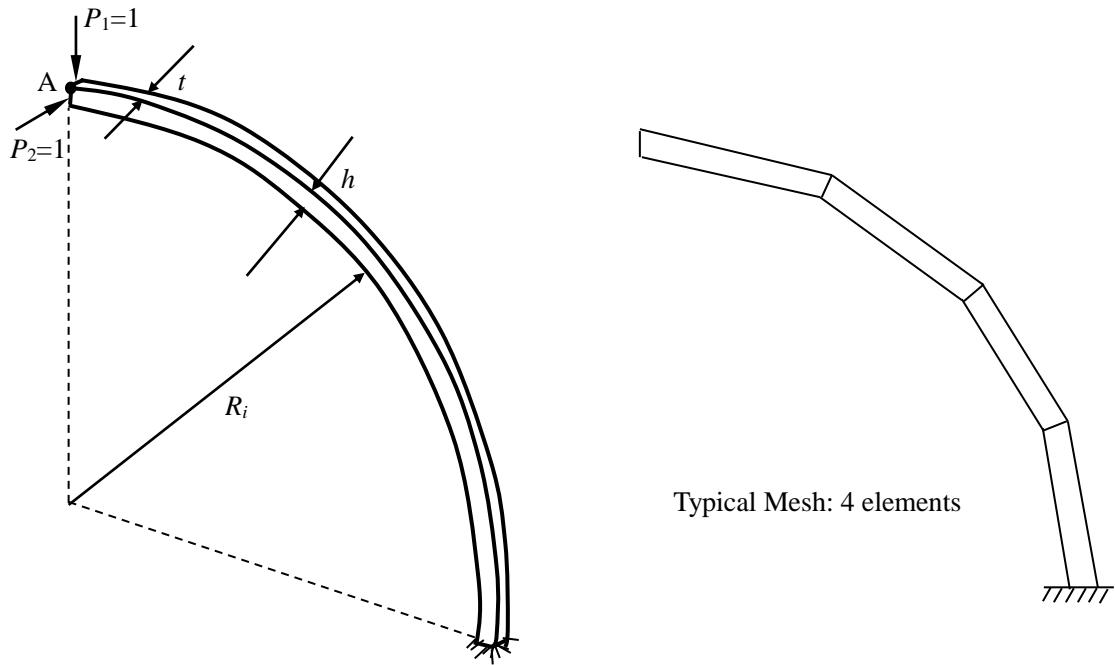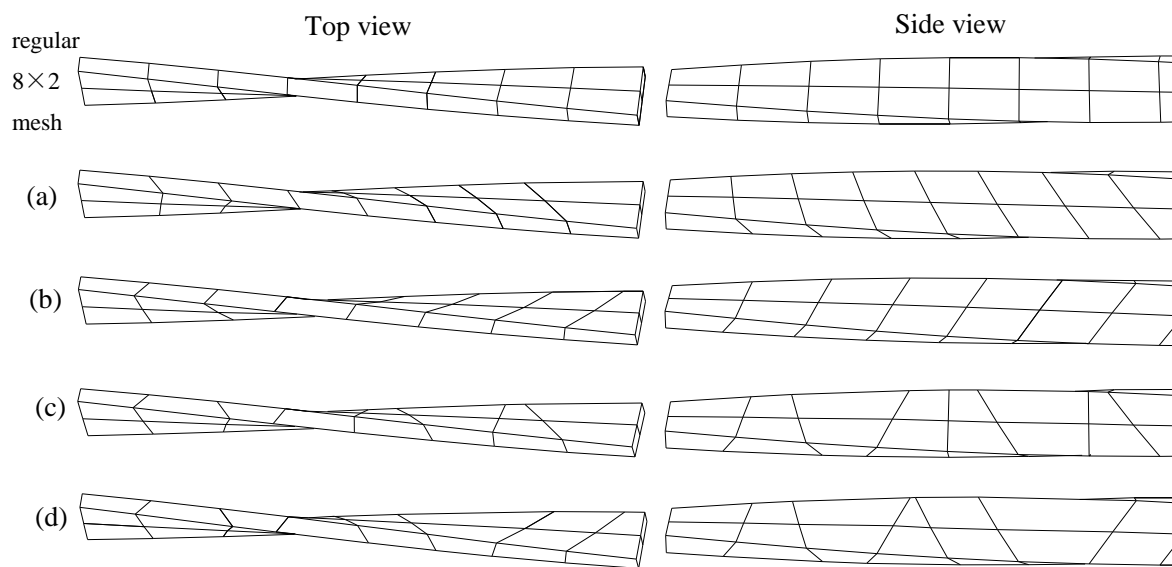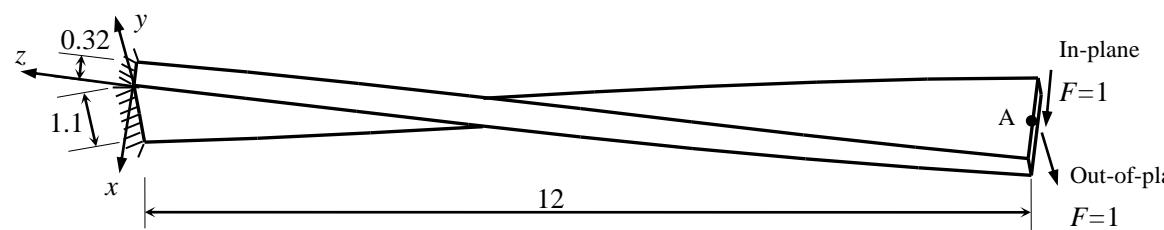
Figure 7. Bending of a thin curved beam.

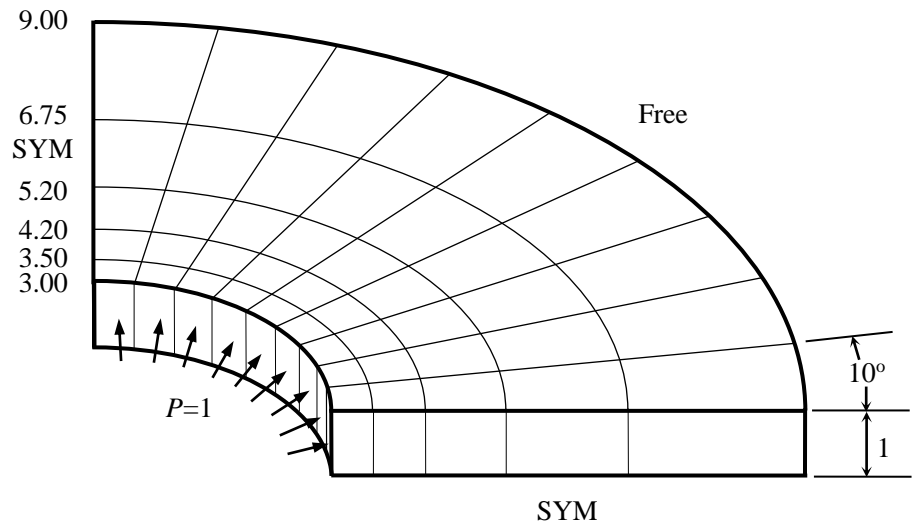Figure 8. Twisted beam problem and meshes. $E=2.9\times10^7$, $\mu=0.22$

Figure 9.   A quarter of thick-walled cylinder and mesh division.